Space Sci Rev (2018) 214:98
https://doi.org/10.1007/s11214-018-0527-0

Dust Phenomena Relating to Airless Bodies

J.R. Szalay[1] · A.R. Poppe[2] · J. Agarwal[3] · D. Britt[4] · I. Belskaya[5] · M. Horányi[6] · T. Nakamura[7] · M. Sachse[8] · F. Spahn[8]

Received: 8 August 2017 / Accepted: 10 July 2018 / Published online: 7 August 2018

Abstract Airless bodies are directly exposed to ambient plasma and meteoroid fluxes, making them characteristically different from bodies whose dense atmospheres protect their surfaces from such fluxes. Direct exposure to plasma and meteoroids has important consequences for the formation and evolution of planetary surfaces, including altering chemical makeup and optical properties, generating neutral gas and/or dust exospheres, and leading to the generation of circumplanetary and interplanetary dust grain populations. In the past two decades, there have been many advancements in our understanding of airless bodies and their interaction with various dust populations. In this paper, we describe relevant dust phenomena on the surface and in the vicinity of airless bodies over a broad range of scale sizes from $\sim 10^{-3}$ km to $\sim 10^{3}$ km, with a focus on recent developments in this field.

Keywords Dust · Airless bodies · Interplanetary dust

Cosmic Dust from the Laboratory to the Stars
Edited by Rafael Rodrigo, Jürgen Blum, Hsiang-Wen Hsu, Detlef Koschny, Anny-Chantal Levasseur-Regourd, Jesús Martín-Pintado, Veerle Sterken and Andrew Westphal

✉ J.R. Szalay
jszalay@princeton.edu

A.R. Poppe
poppe@ssl.berkeley.edu

1 Department of Astrophysical Sciences, Princeton University, Princeton, NJ 08540, USA

2 Space Sciences Laboratory, U.C. Berkeley, Berkeley, CA, USA

3 Max Planck Institute for Solar System Research, Göttingen, Germany

4 University of Central Florida, Orlando, FL 32816, USA

5 Institute of Astronomy, V.N. Karazin Kharkiv National University, Kharkiv, Ukraine

6 Department of Physics, University of Colorado Boulder, Boulder, CO, USA

7 Division of Earth and Planetary Materials Science, Tohoku University, Miyagi, Japan

8 Institut für Physik und Astronomie, Universität Potsdam, Potsdam, Germany

1 Introduction

The term "airless body" refers to any object in the solar system without a global, collisional atmosphere. These bodies comprise a diverse class of objects with great variation in size, shape, surface properties, composition, and orbital characteristics. The interaction between these bodies and their dust environment is complex and occurs on many spatial and temporal scales. Dust is pervasive throughout the observable universe; it comprises the building blocks of all planetary bodies, which are formed from the accretion of dust particles aggregating into much larger objects (Birnstiel et al. 2012; Levison et al. 2015). While dust particles impacting airless bodies at very low speeds contribute to their mass through accretion, high speed impacts can liberate orders of magnitude more mass than the impacting particle and a fraction of those ejecta particles may escape the target bodies' gravity wells. In this way, all airless bodies can be both sources and sinks of dust grains.

This review focuses on dust phenomena relating to airless bodies, highlighting recent advancements in our understanding of such phenomena in the last two decades. To highlight the diverse nature of these objects and frame the subsequent discussions, we begin the review by describing the orbital distribution of airless bodies in the solar system in Sect. 2. We continue by describing dust evolution on airless surfaces and proceed with subsequent sections ordered phenomenologically outward from the surface. In Sect. 3, we summarize the current understanding of how dust on the surface of an airless body evolves and highlight recent asteroidal regolith sample return analyses. In Sect. 4, we specifically describe processes related to meteoroid bombardment, such as impact gardening, exospheric generation, and surface contamination. A global, direct consequence of meteoroid bombardment is the formation of ejecta clouds, and is discussed in depth in Sect. 5. Escaping, unbound ejecta becomes a source of planetary or interplanetary meteoroids and is the focus of Sect. 6. We briefly address electrostatic effects on surface processes in Sect. 7. Finally, we conclude in Sect. 8 with a summary of current open questions and discuss future dust measurements.

2 Orbital Distribution of Airless Bodies

To highlight the diverse nature of airless bodies, here we describe their orbital distribution in the solar system. Airless bodies can be divided into three groups: airless planets, airless moons, and small bodies (e.g. asteroids and comets). For small airless bodies throughout the solar system, there are three reservoirs that are dynamically stable over the age of the solar system: (1) the main Asteroid Belt between Mars and Jupiter; (2) the Jupiter Trojans clustered in the L4 and L5 Lagrangian points of Jupiter's orbit; and (3) the Trans Neptunian Objects (TNOs) outside the orbit of Neptune. These reservoirs contribute bodies to the transitional classes, which include the Near Earth Objects (NEOs) and Centaurs, which consist of bodies that have been perturbed from the stable reservoirs into short-lived planet crossing orbits. When perturbed even further into orbits crossing the inner solar system, Centaurs can develop into comets.

Small bodies orbiting the Sun in the inner solar system are typically classified as either comets or asteroids via three separate criteria: 1) activity, via the detection of observable atmospheres; 2) ice content; and 3) the Tisserand parameter, $T_J = \frac{a_J}{a} + 2\sqrt{((1-e^2)\frac{a}{a_J})}\cos i$, where a, e, i and the semi-major axis, eccentricity, and inclination of the body and Jupiter, denoted by subscript "J" (Jewitt 2012). Comets typically have high activity levels, are predominantly composed of icy materials, and have $T_J < 3$. Asteroids, on the other hand, typically have lower levels of activity, are more rocky, and have $T_J > 3$. The discrimination

between comets and asteroids is not entirely precise, as will be discussed in Sect. 6.2.2 for the case of active asteroids. See review by Jewitt (2012) for a comprehensive description of these criteria.

All of these dynamical reservoirs are essentially survivors of the small bodies in the solar system's original accretion disk that subsequently formed the terrestrial and gas giant planets. These populations have been modified, migrated, and depleted not only by accretion onto the planets and impacts with other small bodies, but also by orbital disruption from gravitational resonances with the giant planets and giant planet orbital migration (Morbidelli et al. 2015). This section provides a brief description of the dynamical classes of airless bodies along with their history. As there is an entire review paper dedicated to comets in this Topical Collection, we omit discussion of cometary-specific processes in this paper.

2.1 Dynamical Classes and Origin of Airless Bodies

2.1.1 Near-Earth Objects (NEOs)

NEO's are a population of relatively small asteroids and comets that have been perturbed by dynamical processes into short-lived orbits that cross the paths of the inner planets (Gladman et al. 2000). The largest NEO is the $\sim$ 32 km diameter (1036) Ganymed and is joined by approximately 1000 objects larger than 1 km diameter. In total, there are probably over 1 million NEOs greater than 40 meters in diameter (DeMeo et al. 2015b). These objects are dominated by chaotic interactions with the inner planets and as a result this is a transitory population with mean lifetimes of approximately 10 million years (Gladman et al. 2000). The population is being constantly replenished by a flux of bodies perturbed from the main asteroid belt, primarily through orbital resonances with Jupiter. Gravitational interactions with Jupiter can rapidly excite the orbit of the small body, increasing its eccentricity until it becomes planet crossing. Early in the study of the asteroid belt it was observed that the dynamical resonance zones called the Kirkwood gaps were remarkably clear of asteroids. Small bodies are moved into the Kirkwood gaps by several processes including collisions with other asteroids and, for objects on the order of a kilometer or smaller, by the Yarkovsky effect (Bottke et al. 2002). As a result, the NEOs effectively sample the zones of the main asteroid belt close to the major resonance zones of the inner asteroid belt.

2.1.2 Main Asteroid Belt

The main asteroid belt lies between 2–4 AU and is probably a strongly depleted and collisionally evolved remnant of what was likely a much more massive population of small bodies (Morbidelli et al. 2015). The current total mass of the asteroid belt is approximately 10^{-4} Earth masses. The presence of Jupiter is the driving force in the structure of the asteroid belt; perturbations from Jupiter early in the solar system formation era limited planetesimal growth and cleared out almost all asteroids within two AU of Jupiter. Orbital mean motion resonances with Jupiter have opened up the Kirkwood gaps and continue to perturb and deplete the asteroid belt, either into the inner solar system or into orbits that interact with Jupiter and are eventually ejected from the solar system. Because of the relatively high eccentricities of asteroidal orbits, collisions are relatively frequent (Morbidelli et al. 2010). Catastrophic collisions between large objects can produce clouds of fragments that are dynamically related. These fragments form the roughly 120 collisional families of the asteroid belt (Masiero et al. 2013; Nesvorný et al. 2015). Differences in thermal inertia observations of main belt asteroids suggest there is a major transition at 100 km diameter in the total dust

content of these objects. Smaller asteroids tend to be similar to the NEOs and show rocky surfaces, while larger asteroids tend to have very small thermal inertias indicating that they are even dustier than the Earth's moon (Delbo et al. 2015).

2.1.3 Jupiter Trojans

These objects are a large population of asteroids trapped in the L4 and L5 Lagrangian points which lead and trail Jupiter in its orbit by 60 degrees. The orbits slowly librate around these points and are characterized by high inclinations. These zones are affected by a number of weak resonances with Jupiter and Saturn which induce chaotic orbital behavior over the age of the solar system (e.g., Levison et al. 1997; Marzari et al. 2003; de Elía and Brunini 2007). Jupiter Trojans can transiently become temporary satellites of Jupiter or join the population of Jupiter family comets. The populations in both zones are roughly similar with about 60,000 objects larger than 2 km (Yoshida and Nakamura 2005). Jupiter Trojans are thought to have two possible origins: (1) during the runaway, accretionary growth of Jupiter, the rapid increase of Jupiter's gravity cause planetesimals that were in or near the Jovian orbit to become trapped in the Trojan zones, or (2) Jupiter Trojans were captured during the migration of the giant planets 500–600 million years after the solar system formation (Morbidelli et al. 2015). Migration during this period greatly disrupted the population of small bodies around the solar system, probably causing the heavy bombardment seen on the Moon and greatly increasing the flux of scattered planet crossing small bodies.

2.1.4 Centaurs

These objects are a transitional group of small bodies that orbit between Jupiter and Neptune. Centaurs have their origins from TNOs that are perturbed onto planet-crossing orbits that are not protected by orbital resonances (Horner et al. 2004). These orbits are chaotic from multiple gravitational encounters with the giant plants and are unstable on a timescale of 10^6–10^7 years. Centaurs evolve into Jupiter-family comets or are ejected from the solar system by encounters with Jupiter (Morbidelli et al. 2015).

2.1.5 Trans-Neptunian Objects

TNOs are a general term for any object beyond the orbit of Neptune and includes the Kuiper belt, scattered disk, and Oort cloud. The Kuiper Belt and the scattered disk probably formed as the result of the migration of the gas giants (Levison et al. 2008). The Oort cloud was filled from small bodies ejected by Jupiter into long elliptic or parabolic orbits during the early stages of solar system accretion. Since the Oort cloud extends over 50,000 AU from the Sun, an additional source of material is from an exchange of ejected small bodies between the Sun and its sibling stars in a stellar cluster during the earliest days of solar system formation (Morbidelli et al. 2008). TNO reservoirs contribute objects to the inner solar system from a number of processes. Objects in the Oort Cloud are perturbed by gravitational interactions with passing stars and molecular clouds in Milky Way. This is probably the source of long-period and Halley-family comets as well as at least some of the Centaurs and Jupiter-family comets (Levison et al. 2008). The scattered disk, because of its interactions with Neptune, high orbital eccentricities, and high inclinations is dynamically less stable and the likely origin for most periodic comets. The Kuiper Belt, on the other hand, is dynamically stable and only rarely contributes objects to planet crossing orbits.

2.1.6 Mercury and Moons

The final category of airless bodies includes the airless planet Mercury as well as numerous moons in the solar system. Origins depend upon the accretionary and chaotic processes of early solar system formation. While Mercury formed from the accretionary disk of the solar nebula, the giant planet large moons probably formed from accretionary discs that formed around these large gravitational concentrations. Other large moons formed from major impacts on the primary (Earth and Pluto). The numerous small moons of the giant planets have their origins either from collisional fragments of previous moons or from small bodies captured during giant planet migration (Nesvorný et al. 2014).

3 Evolution of Dust on Surfaces of Airless Bodies

The surfaces of airless bodies are covered by granular materials called regolith. The term 'regolith' comes from the Greek *rhegos* (blanket) + *lithos* (stone) and is defined by the Glossary of Geology as, "A general term for the layer or mantle of fragmental and unconsolidated rock material, whether residual or transported and of highly varied character, that nearly everywhere overlies bedrock. It includes rock debris of all kinds" (Jackson 1997). In planetary studies, the term regolith is usually used in a broader sense meaning a loose unconsolidated material of the upper surface of a planetary body, including icy bodies. The thickness, texture, particle size, distribution, chemistry, and evolution of regolith depends strongly on the geologic context of the body. The creation and depletion of regolith is driven by weathering processes, including from the meteoroid, thermal, and energetic particle environments.

The best studied example is the lunar regolith, which consists of a very loose, fluffy powder about 20 cm deep overlying a fine-grained and more compact layer that can vary between 4–10 meters in depth (Taylor 1982). This loose layer is in equilibrium between processes that disaggregate particles such as thermal shock and meteoroid bombardment, and processes that fuse particles together such as melting. Below the regolith layer is the so-called megaregolith, which consists of a deep shattered layer of large scale impact ejecta (roughly 2 km thick), structurally disturbed and displaced crust (again from impacts, up to 10 km thick), and finally in situ fractured crust down to 25 km depth (Taylor 1982).

3.1 Regolith Evolution due to Space Weathering

All airless surfaces undergo space weathering, defined as the physical, mineralogical, and chemical alterations suffered by solid materials when exposed to the space environment. This includes a broad range of processes that are fundamentally driven by energetic processes such as impacts, radiation, and the solar wind. The effects of space weathering depend on the chemistry and crystal structure of the target material. Here we briefly review the major components of space weathering and their implications for the regoliths of airless bodies, which are graphically summarized in Fig. 1.

Comminution is the physical process of breaking of rocks and minerals into smaller particles; it is the primary process by which dust is generated on airless bodies. In space this can occur in several ways. Impacts at all scales grind down particle size. Major impacts that do not completely disrupt the parent body (e.g., Asphaug et al. 1998; Michel et al. 2003; Goodrich et al. 2004) produce ejecta blocks and fracture the bedrock, while meteoroids grind down gravel and blocks to dust. For objects in interplanetary space (as opposed

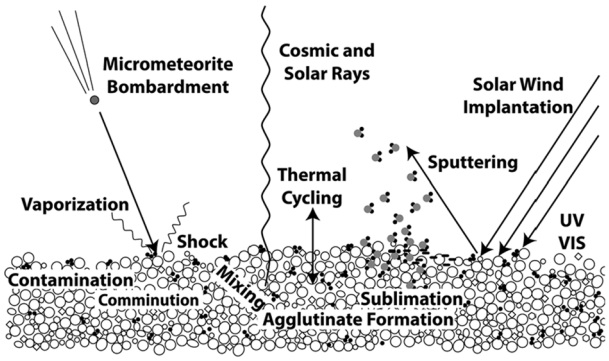

Fig. 1 A summary of the many space weathering processes occurring on airless bodies. *Reproduced from Pieters and Noble (2016) with permission from the Journal of Geophysical Research*

to objects within planetary gravity wells), this effect is a function of heliocentric distance with meteoroid impact velocities dropping off rapidly with distance. Another comminution process is thermal fracturing. In the inner solar system, strong solar heating on the sunward side of rotating asteroids followed by sudden cooling on the dark side, produces substantial thermal shock due to either the different thermal expansion characteristics of the constituent minerals or the thermal gradient within a homogeneous rock which leads to tensile stress between the outer and inner layers. This thermal shock has been shown to propagate fractures in meteorites and, in the inner solar system, can rapidly disaggregate materials (Delbo et al. 2014). This effect is a strong function of heliocentric distance since it depends upon solar heating. These comminution processes push airless surfaces to accumulate fine-grained dust which is seen, for example, in the powdery lunar soil (Hapke 2001).

Dust accumulation, however, is also a strong function of local gravity and heliocentric distance. For small asteroids with low gravity and hence, low escape velocity, a significant portion of impact ejecta will escape the body. Thermal inertia studies show that smaller asteroids are fundamentally coarser grained and rockier than larger asteroids (Delbo et al. 2015). For small near-Earth asteroids, electrostatic interactions may preferentially shed small grains, making the surfaces of these objects even rockier than similar sized bodies in the asteroid belt, since both UV and plasma fluxes decrease with the square of heliocentric distance (Lee 1996). Another hypothesis is that the large surface roughness on small asteroids is caused by the inwards migration of regolith fines due to the Brazil Nut Effect (e.g. Perera et al. 2016).

Acting against comminution is agglutination. Agglutination is the process of melting and welding mineral and rock fragments together by micrometeorite-impact-produced glass. The primary example of agglutination are the high velocity impacts into lunar soil that produce enough heating to melt or vaporize material and weld fragments back together (Taylor 1982). This process is present at the Moon and Mercury, since impacts are energetic enough for the required melting and vaporization; however, it may also be relevant for satellites deep within the gravity wells of the large outer planets. Agglutinates are only rarely found in meteorites because average impact velocities in the asteroid belt are too low to produce extensive melting. Since agglutination welds particles together, it competes with the generation of dust by comminution. Over time, an equilibrium develops where comminution is balanced by agglutination.

In addition to kinetic energy inputs from impacts, energy can also be delivered by a range of processes associated with radiation and the solar wind (Brunetto et al. 2015). Without an atmosphere, solar system materials on airless bodies are directly subjected to the cosmic and solar particle environment. Electrons and ions can carry substantial energy flux and change

the chemical environment of surfaces to which they are exposed. Energetic solar and galactic cosmic rays can penetrate minerals and cause crystal damage, producing dislocations and dangling bonds that make crystal structures more disordered and potentially more reactive. Cosmic ray spallation is a result of the collision between an energetic cosmic ray particle and a nucleus, which results in the modification of the atomic makeup of surface elements. This changes the elemental chemistry of the target atom and, because of nuclear interactions with the cloud of ejected nuclear particles, potentially the elemental chemistry of surrounding atoms. Sputtering is a slightly less energetic process, whereby atoms are ejected from the target material due to bombardment by thermal and supra thermal ions (Biersack and Eckstein 1984; Berisch and Eckstein 2007). The sputtered atoms mostly recondense on nearby grain surfaces but the general trend is to increase crystal disorder, disrupt crystal structure, and create amorphous rims of recondensed material (e.g., Christoffersen et al. 1996; Keller and McKay 1997; Carrez et al. 2002; Keller and Berger 2014; Matsumoto et al. 2015; Poppe et al. 2018). Airless bodies are typically effective cold traps for the recondensing vaporized material.

For terrestrial bodies, the net effect of space weathering from charged particle irradiation and meteoroid bombardment is to both darken and redden the surface (e.g., Pieters et al. 1993, 1994; Noble et al. 2007; Pieters and Noble 2016). Many airless bodies are directly exposed to the solar wind, which is composed of approximately 97% protons (H^+) and 3% alpha particles (He^{++}) at typical speeds of 420 km/s (Dmitriev et al. 2011). Solar wind material is implanted in the surfaces and shallow interiors of exposed regolith. The fundamental chemical implication of solar wind implantation is to set up a chemical disequilibrium between the reducing veneer of the solar wind hydrogen and the oxidized silicates that make up airless bodies, adding to the already low oxygen fugacity of the hard space vacuum. This chemical disequilibrium can persist as long as temperatures are low enough to preclude any rapid reactions; however, if the regolith material is heated by, for example, a meteoroid impact, then the implanted hydrogen can drive reduction reactions in the silicates. These reactions convert iron-rich silicates into elemental iron and iron-poor silicates, producing nanophase iron (npFe) particles often found suspended in the agglutinitic glass of lunar regolith (Noble et al. 2007). These npFe particles are a source of one of the characteristics of space weathering, namely, the very strong red slope in lunar reflectance spectra (Pieters and Noble 2016).

While both charged particle irradiation and meteoroid bombardment play a role in space weathering as a whole, the relative importance of these two processes remains uncertain. Furthermore, the rates of irradiation and bombardment may actually change as a function of heliocentric distance, as fluxes and velocity distributions of both interplanetary dust grains and ambient charged particles change. For example, spectra obtained at Mercury are consistent with both an overall greater amount of sub-microscopic iron and a higher ratio of larger (> 50 nm) to smaller (< 50 nm) iron particles than at the Moon, which is attributed to increased production of impact vapor and melt due to meteoroid bombardment at Mercury (Lucey and Riner 2011). This is furthermore consistent with the expected increase in impact velocities of meteoroids at Mercury given its smaller heliocentric distance (Cintala 1992; Hahn et al. 2002). Other optical effects of weathering are more subtle. On asteroids, weathering creates crystal damage in silicates and decreases spectral contrast, which darkens reflectance spectra and shallows absorption bands. Shock can also redistribute the particle size of opaques in asteroid material, resulting in increased darkening (Britt and Pieters 1994).

Space weathering by meteoroid impacts in the outer solar system likely takes on a different character than in the inner solar system due to the predominantly icy surface compositions of outer solar system bodies. For example, many icy surfaces in the outer solar system

are in the form of crystalline water ice rather than amorphous solid water (e.g., Grundy et al. 1999; Brown and Calvin 2000; Jewitt and Luu 2004; Merlin et al. 2007; Trujillo et al. 2007; Dalle Ore et al. 2015; Terai et al. 2016). Amorphous solid water would typically be expected given the relatively cold temperatures in the outer solar system and amorphizing processes such as proton and energetic ion irradiation (e.g., Jenniskens and Blake 1996; Leto and Baratta 2003; Mastrapa and Brown 2006). The formation of crystalline water ice requires either fresh deposition of water ice (i.e. via cryovolcanism; e.g., Jewitt and Luu 2004; Cook et al. 2007; Desch et al. 2009; Desch and Neveu 2017) or a source of external heat to transform the amorphous ice into a crystalline state. While one possible source of external heat is from large-scale impacts (e.g., Dalle Ore et al. 2015), meteoroid bombardment may play a role in producing crystalline water ice on planetary surfaces in the outer solar system (Porter et al. 2010). Annealing via meteoroid bombardment has also been suggested as an active process in extrasolar debris disks that display evidence of crystalline water ice signatures (McClure et al. 2015).

3.2 Laboratory Studies of Dust Samples from Airless Bodies

Given the complexity of processes occurring on regolith that covers airless bodies, the ability to examine actual samples of this material in a laboratory setting is extremely valuable. However, returning regolith samples from airless bodies is a challenging endeavor and has only been performed on a small number of airless bodies in the solar system.

The Apollo lunar sample returns revolutionized our understanding of space weathering processes occurring on the lunar surface, and have served as an analogue for weathering processes on many other airless bodies. Our understanding of most of the concepts outlined in the previous section evolved dramatically due to these lunar sample returns and their subsequent analysis via Earth-based techniques. There is large body of literature covering a multitude of lunar regolith topics. Comprehensive reviews on space weathering are given in Hapke (2001) and Pieters and Noble (2016), for example. For detailed discussion of the lunar mare soils, nanophase iron, and particle size distributions, see for example Taylor et al. (2001), Park et al. (2008), Liu et al. (2008), Taylor et al. (2010), Liu and Taylor (2011). In this section, we focus on the more recent Itokawa mission, which returned the first asteroidal regolith sample to Earth, allowing for direct comparisons between the lunar regolith and that of a much smaller airless body at 1 AU.

In September 2005, the Japanese Hayabusa spacecraft visited 25143 Itokawa (Fujiwara et al. 2006), an S(IV)-type, ellipsoidal ($500 \times 294 \times 209$ m) asteroid on an Apollo and Mars-crossing orbit. Itokawa was found to be covered with boulders that have a variety of sizes and morphologies. The current shape of Itokawa suggests it is a rubble pile asteroid comprised of reassembled pieces of a much larger parent asteroid (about 20 km in radius), which most likely broke up due to a catastrophic impact (Fujiwara et al. 2006; Nakamura et al. 2011). One smooth area, MUSES-C Regio, was found at the center of the asteroid (Yano et al. 2006). Hayabusa landed twice on the MUSES-C Regio to collect dust particles. In June 2010, Hayabusa returned to the Earth with a sample of < 1 g of Itokawa dust particles in a recovery capsule, allowing for their study and characterization in a terrestrial laboratory setting. Of the recovered particles, the largest are several hundred microns, while most are smaller than 10 μm in diameter (Nakamura et al. 2011). The size distribution and morphology of the particles suggest that meteoroid impacts on the asteroid surface is the primary source of these regolith particles, and that seismic-induced grain motion in the smooth terrain abrades them over time (Tsuchiyama et al. 2011). Itokawa particles retain morphological and isotopic evidence suggestive of a dynamic asteroidal regolith environment.

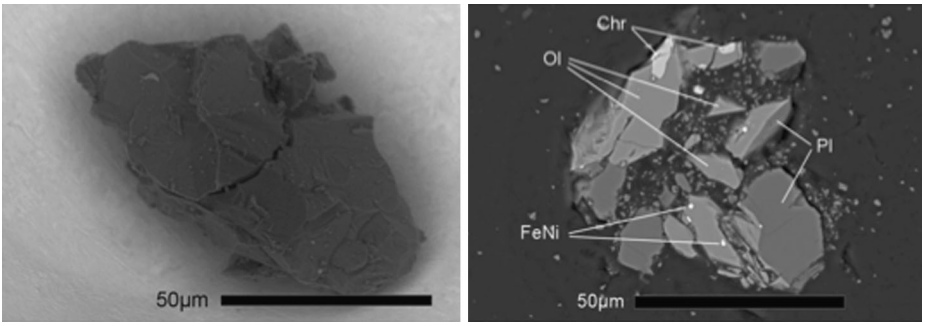

Fig. 2 Regolith particle RA-QD02-0242 recovered from MUSES-C Regio of asteroid 25143 Itokawa. (**a**) The particle shows edged morphology and contains some large cracks, suggesting that it is an impact-fragmented piece of a larger rock. (**b**) Cross section of the particle shows that it consists of well crystalline olivine (Ol), plagioclase (Pl), chromite (Chr), and FeNi metal (FeNi). Large cracks go through the entire particle

A typical particle (Fig. 2) consists mainly of anhydrous silicates such as olivine, low and high Ca pyroxene, and plagioclase with chemical compositions similar to LL ordinary chondrites, indicating S-type asteroids are parent objects of ordinary chondrites, which are the most abundant meteorites recovered on Earth (Nakamura et al. 2011). Most particles showed mineralogical evidence of long-term thermal metamorphism. The peak temperature of the metamorphism was around 800 °C based on pyroxene thermometry (Nakamura et al. 2011). The short-lived radionuclide ^{26}Al was probably a major heat source when Itokawa's parent body formed in the early solar system. At $\sim$ 5 million years after the formation of calcium-aluminum-rich inclusions (CAI) at various depths, the asteroid experienced its maximum temperature and subsequently slowly cooled down. Thermally-metamorphosed particles were initially formed deep inside of the asteroid, but excavated and deposited on the newly accreted body after the putative impact event. Ar-Ar dating of several particles implies that the final disrupting catastrophic impact occurred around 1.3 Gyr ago (Park et al. 2015).

Analysis of the recovered particles showed high concentrations of light solar wind noble gases (Nagao et al. 2011). High resolution electron-microscope observations indicated that a thin layer of Fe-rich nanoparticles developed at the surface of ferromagnesian silicates, which suggests reduction of FeO in silicates by solar wind protons (Noguchi et al. 2011). Some particles showed vapor deposition of sulfur-bearing Fe-rich nanoparticles on the surface, suggestive of sputtering of FeS from nearby minerals (Noguchi et al. 2011). Meteoroid impacts on the surface of regolith produced microcraters and melt splashes on particle surfaces that are similar to those found in lunar soils (Nakamura et al. 2012). The residence time of regolith particles can be estimated from concentrations of spallogenic noble gases that were produced in the particles during exposure to galactic cosmic rays. Low concentrations of noble gases suggest the particles had relatively short residence times of $<$ 8 million years at $<$ 1 m depth (Nagao et al. 2011). This implies loss of small dust particles from Itokawa's surface due to low gravity and therefore suggests continuous surface depletion and refreshment over time.

A wealth of information has already been garnered from the Itokawa sample return, allowing for characterization of asteroidal regolith in a manner only possible with advanced ground-based laboratory techniques. This sample will continue to provide insight into asteroidal evolutionary processes for decades to come. Future asteroidal missions, such as OSIRIS-REx (Lauretta et al. 2015) and Hayabusa-2 (Yoshikawa et al. 2011), aim to return

samples from their respective targets. These missions would further diversify our asteroidal sample set and greatly improve our understanding of asteroidal surface and dust grain evolution.

3.3 Remote-Based Estimations of Regolith Depth and Particle Size

While asteroidal samples allow for highly sophisticated laboratory techniques to analyze the surface of an asteroid, acquiring such samples is challenging. Many remote-based techniques have been developed, such as phase-resolved photometry and polarimetry, to characterize regolith properties by more indirect methods. Measurements of phase angle effects in brightness and polarization give a first look into the top-most surface properties. Optical polarization parameters of the lunar surface, asteroids, Centaurs, and TNOs are found to be quite varied (see reviews by Shkuratov et al. 2011; Belskaya and Bagnulo 2015; Belskaya et al. 2015). These polarization differences, as well as observations of thermal inertia (e.g., Gundlach and Blum 2013), have been interpreted to suggest the average size of asteroid regolith particles is greater than that of lunar regolith particles. For example, the Moon and Mercury were found to have small average particle sizes on the order of 10's of μm, while smaller bodies like the Martian moons Phobos and Deimos, as well as other asteroids of similar sizes to those moons were found to have larger average particles sizes on the order of 1–10's mm (Gundlach and Blum 2013). The polarization properties of the surfaces of TNOs and Centaurs also suggests the presence of a thin frost layer of sub-micron particles (Belskaya et al. 2010).

The values of thermal inertia determined from infrared measurements provide insight into the thickness and texture of the regolith layer on the surfaces of airless bodies. It was found that the thermal inertia of asteroids typically increases substantially with decreasing size, suggesting different regolith properties between large asteroids and small objects without the gravity necessary to retain fine regolith fragments generated by impacts (Delbo et al. 2015). Measurements of thermal inertia of TNOs are 2–3 orders of magnitude lower than expected for compact ices and suggest highly porous surfaces (Lellouch et al. 2013).

More detailed information on regolith properties can be obtained from analysis of crater morphology using high-resolution images taken close to a planetary body. Recent space missions to several asteroids have revealed complex dynamics of regolith on their surfaces (see Murdoch et al. 2015 for a review). The depth of the regolith layer was estimated as $\sim$ 600–800 m for the large asteroids 4 Vesta and 21 Lutetia and less than 50 m for smaller size asteroids (433 Eros, 243 Ida).

4 Meteoroid Bombardment

Meteoroid bombardment of planetary surfaces by interplanetary and planetary dust grains is a major driver of various processes that shape and influence the surfaces of airless bodies throughout the solar system. These processes include the vaporization and melting of surface material, the injection of neutral atoms and molecules into exospheres or coronae, the production of micron and sub-micron sized ejecta, and the compositional modification of the surface material via the introduction of exogenous material.

4.1 Meteoroid Fluxes onto Airless Bodies

Fluxes of meteoroids that contribute to the bombardment of airless surfaces originate from three main sources: planetary, interplanetary, and interstellar. Planetary dust grains originate

from bodies within the gravity well of a parent planet or object. Examples of this include the massive Phoebe ring at Saturn (Verbiscer et al. 2009; Hamilton et al. 2015), the active plumes of Enceladus (Spahn et al. 2006; Porco et al. 2006), and theoretically, the minor moons of the Pluto-Charon system (Thiessenhusen et al. 2002; Poppe and Horányi 2011; Pires dos Santos et al. 2013). The resulting mass fluxes from any of these various sources can be highly dependent on the dynamical details specific to any system.

Interplanetary dust grains (discussed in detail in the Interplanetary Dust review) are typically the main source of impacting meteoroids for airless bodies throughout the solar system. In the inner solar system, the dust complex is thought to be dominantly formed by cometary dust originating from Jupiter-family comets (e.g., Nesvorný et al. 2010; Nesvorný et al. 2011a) with additional contributions from both asteroids and longer period comets such as Halley type and Oort Cloud comets (Wiegert et al. 2009; Nesvorný et al. 2011b; Pokorný et al. 2014). These fluxes are typically dominated by the sporadic component of the interplanetary background, whose grains experience a significantly different evolution than their parent object such that any dynamical link is erased (Jones and Brown 1993). However, meteoroid showers can be dominant over short periods of time at an airless body (e.g., Killen and Hahn 2015; Colaprete et al. 2016; Szalay and Horányi 2016a).

In the outer solar system, dust grains originate from four main sources: Jupiter-family comets (also the main source for the inner solar system), Halley-type comets, Oort Cloud comets, and Edgeworth-Kuiper Belt objects (e.g. Poppe 2016). Modeling of the equilibrium dust distributions in the outer solar system has suggested varying degrees of contribution from each of these sources, with Jupiter-family cometary dust dominating near Jupiter, Oort Cloud cometary dust dominating between Saturn and Neptune, and Edgeworth-Kuiper Belt grains dominating from Neptune outwards (e.g., Liou and Zook 1999; Vitense et al. 2012; Poppe 2016). At Jupiter, interplanetary dust mass fluxes are on the order of 10^{-13} g m^{-2} s^{-1} (Sremčević et al. 2005), tapering off to approximately 10^{-14} g m^{-2} s^{-1} between 10 and 50 AU (with a slight enhancement in the Edgeworth-Kuiper Belt between 30–45 AU) (Poppe 2016).

Finally, interstellar grains flow through the entire solar system due to the relative motion between our solar system and the local interstellar cloud (e.g., Grün et al. 1994; Mann 2010; Sterken et al. 2012, 2015; Strub et al. 2015; Krüger et al. 2015). The typical mass flux of interstellar dust grains is $\approx 5 \times 10^{-17}$ g m^{-2} s^{-1}, several orders-of-magnitude less than interplanetary dust; however, at far heliocentric distances where the IDP impact speeds will be on the order of a few km/s, the relatively high velocity of interstellar grains (≈ 26 km/s) implies that interstellar grains may still be an important source for processes that scale strongly with impact velocity.

4.2 Gravitational Focusing

Gravitational focusing, the process by which the speed, density, and flux of a stream of particles is increased in the vicinity of a central mass such as a planet, is an important phenomenon when considering the bombardment of planetary surfaces. Particles that enter the Hill sphere of an object are accelerated towards the attracting mass and, as they are pulled towards the same central point, get closer to each other. The amplification of the impactors' kinematic properties is quantified by focusing factors, each defined as the ratio of a variable at a given distance from the body to its value at infinity. These expressions were first derived by Colombo et al. (1966) with later corrections and independent verification by Spahn et al. (2006b). The focusing factors for the incident particle density n_{imp}, velocity v_{imp}, and flux

$F_{\rm imp}$, relative to their values at infinity ($n_{\rm imp}^{\infty}$, $v_{\rm imp}^{\infty}$, and $F_{\rm imp}^{\infty}$, respectively) are,

$$\frac{v_{\rm imp}}{v_{\rm imp}^{\infty}} = \sqrt{1 + \frac{2GM_{\rm p}}{r(v_{\rm imp}^{\infty})^2}} \tag{1}$$

$$\frac{n_{\rm imp}}{n_{\rm imp}^{\infty}} = 0.5\sqrt{1 + \frac{2GM_{\rm p}}{r(v_{\rm imp}^{\infty})^2}} + 0.5\sqrt{1 + \frac{2GM_{\rm p}}{r(v_{\rm imp}^{\infty})^2} - \left(\frac{R_{\rm p}}{r}\right)^2\left[1 + \frac{2GM_{\rm p}}{R_{\rm p}(v_{\rm imp}^{\infty})^2}\right]} \tag{2}$$

$$\frac{F_{\rm imp}}{F_{\rm imp}^{\infty}} = \frac{v_{\rm imp}}{v_{\rm imp}^{\infty}}\frac{n_{\rm imp}}{n_{\rm imp}^{\infty}}, \tag{3}$$

where G is the gravitational constant, r is the radial distance from the center of the body, and $M_{\rm p}$ and $R_{\rm p}$ are the mass and the radius of the central object (e.g., planet), respectively. Since gravitational focusing is inversely proportional to the impact velocity, it will enhance the magnitude and modify the direction of slow-moving dust population fluxes more than faster populations.

Figure 3 (left) shows these enhancement factors for the Galilean moons as a function of radial distance to illustrate how significant the effect can be for a moon orbiting a large planet. The right panel of Fig. 3 shows the flux enhancement factors for a variety airless bodies in the solar system. At Io, deep inside Jupiter's gravity well, gravitational focusing can increase incident dust grain fluxes up to two orders-of-magnitude. Note that gravitational focusing from satellites themselves is typically negligible compared to the focusing from their parent body. Bodies such as Mercury and the Moon have lower gravitational enhancements than the outer planet moons, due to the shallower gravity wells of Mercury itself and the Earth relative to Jupiter and Saturn. At the Moon, Earth's gravitational enhancement is negligible for impact speeds above a few km/s.

Such an effect can be important when calculating relative fluxes between different populations outside and inside of planetary gravity wells. For example, cometary dust populations typically have greater impact speeds (due to their higher eccentricities) than typical, prograde, heliocentric populations (e.g., Edgeworth-Kuiper Belt dust grains in the outer solar system); however, even if cometary sources may dominate the flux in interplanetary space, gravitational focusing can cause heliocentric populations to be the dominant impactor flux deep within a planetary gravity well (e.g., see Fig. 8, Poppe 2016).

4.3 Impact Gardening

A direct consequence of meteoroid bombardment is impact gardening, whereby impacts stimulate lateral and vertical redistribution of regolith on an airless body. Impact gardening rates were estimated for the Moon based on Apollo sample returns and lunar cores, as well as Monte Carlo models that tracked the movement and redistribution of lunar soil subject to meteoroid impacts (e.g., Gault et al. 1974; Arnold 1975; Morris 1978). Morris (1978) derived an empirical relationship between the gardening (or "reworking") depth, defined as the depth at which there exists a 50% probability of having been gardened by an impact, and time given by $D_R = 2.2t^{0.45}$, where D_R is in units of cm and t is in units of Myr. This rate is fairly significant, implying that a full meter of soil has been gardened over the age of the Moon. Much more recently, Szalay and Horányi (2016b) have estimated the accumulation timescale (i.e., the time period over which the surface is covered by a single layer of impact ejecta) and depth accumulation rate of regolith gardening at the Moon near the equator using data from the Lunar Atmosphere and Dust Environment Explorer (LADEE) mission (Elphic

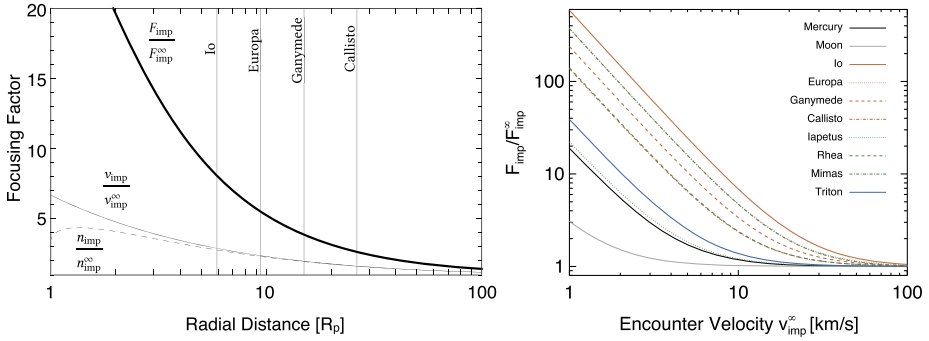

Fig. 3 *Left.* Focusing factors in the Jovian system as a function of distance from the planet for impacts of interplanetary dust particles with $v_{\mathrm{imp}}^{\infty} = 9$ km/s. The thin vertical lines are the positions of the Galilean moons. *Right.* Flux focusing factor for Mercury, the Moon, and a selection of moons of Jupiter (orange), Saturn (green), and Neptune (blue)

et al. 2014) to be approximately 10^4 yrs and 40 µm/Myr, respectively. Analysis of crater production using data from the Lunar Reconnaissance Orbiter (LRO) suggests the top two centimeters are churned every 81,000 yrs (Speyerer et al. 2016). Comparing the LADEE and LRO gardening estimates remains challenging as each estimate addresses different ejecta regimes; LRO images allow for characterization of the redistribution of the low velocity portion of the ejecta, while the LADEE data infers the amount of reblanketing occurring due to particles which are ejected to significantly high altitudes ($\sim$ 1–250 km).

The process of impact gardening will occur on all airless bodies in the solar system in one form or another. At the Moon, which is sufficiently large to retain a large fraction of impact ejecta, meteoroid impacts serve to rework and redistribute the lunar soil to different locations and depths. At smaller bodies, such as the majority of asteroids, impact bombardment will most likely result in a large fraction of ejecta that is unbound and will not return to the surface. In this regime, the impacts directly serve to expose fresh material. The transition between these two regimes is dependent on a variety of factors such as the mass of the body and the speed distribution of impact ejecta. The relative fraction of bound vs. unbound ejecta has been previously estimated for NEAs (Szalay and Horányi 2016c), however, constraints on this ratio for all airless bodies in the solar system have not yet been undertaken.

Impact gardening has important implications for the presence of volatile material known to be sequestered in polar cold traps at Mercury (e.g., Harmon et al. 2011; Neumann et al. 2013), the Moon (Colaprete et al. 2010; Hayne et al. 2015), and Ceres (Platz et al. 2016). Impact vaporization of meteoroids on airless surfaces brings significant amounts of volatile species (e.g., H_2O) (Berezhnoy et al. 2012; Füri et al. 2012) which can be deposited into polar cold traps following migration across the planetary surface. When meteoroid bombardment occurs on the polar cold trapped regions themselves, two processes can occur: (1) ejection and loss or (2) burial and further sequestration of volatile material. Vapor production from meteoroid bombardment is a relatively "hot" process with characteristic temperatures of 2500–5000 K (see Sect. 4.4) and thus, any vaporized material can easily be lost from polar regions. On the other hand, secondary ejecta produced by meteoroid bombardment will be redeposited across the surface and can effectively bury volatile material. Monte Carlo simulations have explored this process at both Mercury and the Moon and found that significant layers of volatile deposits can be buried several meters deep due to

ejecta emplacement from bombardment (e.g., Crider and Vondrak 2003; Crider and Killen 2005; Hurley et al. 2012). Reserves of polar hydrogen have been observed at the Moon, which have survived billions of years of impact gardening, adding further evidence to the notion that impact gardening may help preserve volatile content in the polar regions (Siegler et al. 2016).

4.4 Surface Bounded Exospheres

Meteoroid bombardment is an important source in the production of neutral surface-bounded-exospheres and/or coronae at airless bodies throughout the solar system. Upon impact on a planetary surface, meteoroids can be significantly, if not completely, vaporized, along with varying fractions of the surface material as well (Cintala 1992). Any vaporized material can then be injected onto ballistic or escaping trajectories about the body. Laboratory experiments have quantified the degree of vaporization and the characteristic temperatures of the resulting neutral cloud, finding that the vaporization yield scales as $v^{2.4}$, where v is the impact velocity (Collette et al. 2013, 2014). While the experiments observed a vaporization fraction of 5–10% for the slowest impact velocities (2 km/s), extrapolation of the power-law fit suggested that total vaporization yields equal to and greater than the incoming meteoroid mass (indicating that surface material is also being vaporized in appreciable quantities) occurred for impact velocities greater than approximately 20 km/s. These experiments determined the impact vaporization cloud temperature to be between 2500–5000 K, with a power-law dependence on the impact velocity.

In the inner solar system, surface-bounded exospheres have been detected at Mercury and the Moon (see extensive reviews by Stern 1999; Killen and Ip 1999), and predicted for the moons of Mars (Cipriani et al. 2011; Poppe et al. 2016) and various asteroids (Morgan and Killen 1998; Schläppi et al. 2008). As with impact gardening, the extent to which a surface bounded exosphere exists at an asteroid depends on a variety of factors, such as the mass of the body, the relative sources of elements on the surface available to populate the exosphere, and the speed distribution of outgoing neutrals. Meteoroid bombardment plays an important role, along with charged-particle sputtering, in liberating refractory materials from the surface regolith into the exosphere, including species such as O, Na, K, Al, Mg, Ca, Ti, and Fe (e.g., Sarantos et al. 2012; Colaprete et al. 2016). The spatial and temporal variability of the incident meteoroid bombardment flux is often reflected in the vaporized neutral distributions, as observed at Mercury and the Moon (e.g., Hunten et al. 1998; Smith et al. 1999; Kameda et al. 2009; Killen and Hahn 2015; Szalay et al. 2016; Colaprete et al. 2016; Pokorný et al. 2017), including variations from both the sporadic interplanetary dust background and meteoroid streams (such as the Leonid and Geminid streams). Finally, incoming meteoroids can also serve as a source of exogenous species at airless bodies; for example, meteoroids are believed to introduce approximately 5×10^5 kg/yr of water to the lunar surface, potentially the dominant source of such influx (Füri et al. 2012).

4.5 Surface Contamination

Meteoroid bombardment of airless bodies can also alter the composition of planetary surfaces via the introduction of exogenous material. Perhaps the most striking example of this process is Saturn's moon Iapetus, displayed in Fig. 4, which possesses a hemispherical dichotomy in both color and albedo (Cruikshank et al. 1983). Among various theories, the deposition of dust from Saturn's outer, irregular, retrograde moon Phoebe onto the surface

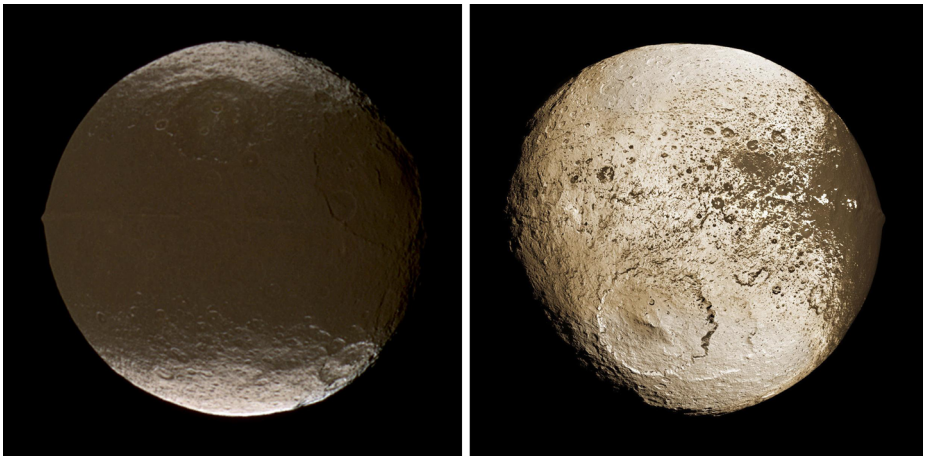

Fig. 4 The leading and trailing hemisphere of the saturnian moon Iapetus, respectively, showing the preferential dark dust deposition on the leading hemisphere. [Courtesy: NASA/JPL/Cassini mission]

of Iapetus stands as the most plausible explanation, especially given the recent discovery of a dust ring around Saturn co-located with Phoebe (Verbiscer et al. 2009). Phoebe's dark and complex surface spectrally matches the dark surface material seen on Iapetus while the bright and icy surface is most likely Iapetus' "true" composition (Clark et al. 2012; Dalle Ore et al. 2012). Dynamical modeling of Phoebe's dust ring and its deposition onto Iapetus strongly supports this hypothesis, with the modeled surface deposition region closely aligning with that observed by Cassini (Tamayo et al. 2011). Surface contamination of satellites is not limited to Iapetus, but seen at most of the mid-sized saturnian icy satellites (Rhea, Dione, Tethys), albeit in far less dramatic fashion (e.g., Clark et al. 2008; Scipioni et al. 2013, 2014). While these satellite surfaces are predominantly (> 99%) water ice, a "dark material" on the order of 1% by composition persists across these moons. Most analyses have suggested that this material is of exogenous origin to the saturnian system, suggesting that material transported into the system from interplanetary dust may be a possible cause (e.g., Mendis and Axford 2008); however, the exact source and method of deposition onto the icy saturnian satellites is not well understood. Dynamical models of dust in the Phoebe ring suggest that while the grains are easily transported to Iapetus (the next major moon inwards of Phoebe), any grains that pass Iapetus are efficiently swept up and/or dispersed from the saturnian system by Titan and thus, unable to reach the inner icy satellites (Tamayo et al. 2011). In contrast, interplanetary dust penetrates throughout the entire saturnian system; however, it is not clear yet that preferential directions in the incoming IDP flux at Saturn (i.e., similar to that suggested at the Galilean satellites (Sremčević et al. 2005)) will yield asymmetric patterns on the inner icy satellites due to the tidally locked nature of these moons. Continued study of dust dynamics and surface contamination of the saturnian satellites, and indeed at all the satellites of the giant planets, is clearly still warranted. Surface material exchange and contamination has also been studied for other multiple satellite systems, including Phobos and Deimos (e.g., Nayak et al. 2016) and the Pluto-Charon system (e.g., Stern 2009; Poppe and Horányi 2011; Porter and Grundy 2015); however, definitive identification of surface ejecta exchange at these multiple satellite systems has not yet been shown.

5 Impact Ejecta Clouds

Ejecta clouds exist in the vicinity of all airless bodies in the solar system due to continual bombardment by fast meteoroids. Comets also experience impact ejecta processes, however, more detailed discussion of additional loss processes at comets is beyond the scope of this review. The impactors are interplanetary dust particles with typical sizes of 1–100 µm (Divine 1993) and typical speeds of a few 10 km/s, particularly after gravitational focusing near a large planet (Colombo et al. 1966; Spahn et al. 2006b). Owing to the impactor's high kinetic energy, the surface of the target is eroded and a cloud of ejecta, typically more numerous and massive than the impactor, is released into space. Depending on the ejection speed and the target mass, the grains either fall back to the surface or they escape the target's gravitational influence and add to the planetary or interplanetary dust environment.

5.1 The Impact Ejection Process

Physically, the impact-ejection process is a combination of an inelastic collision between the impactor and the target, and a fragmentation of the impactor and/or the target. The momentum of the incoming dust particle is conserved and distributed over the ejecta and target, where the target body's velocity is unchanged due to its high mass. However, the impactor's kinetic energy is not conserved and largely (typically $> 70\%$) used to disintegrate and heat the material (Asada 1985; Hartmann 1985). Modeling the impact-ejection process from basic physics is prohibitively complex. Instead, impact-ejection models are based on findings of laboratory experiments (e.g., Koschny and Grün 2001a,b) and on theoretical constraints. Future measurements at high-speed dust accelerators may further elucidate fundamental impact ejection characteristics (Shu et al. 2012).

Given the impactor's mass, speed, and flux at the target, the amount of material ejected by a given impactor can be estimated. Impact experiments show that the volume of the impact crater is a measure for the kinetic energy of the impactor. The relation can be fitted by a power law in the form $V_\mathrm{e} = c_1\, K_\mathrm{imp}^{c_2}$, where the parameters c_1 and c_2 depend on the target material. For impacts on the Jovian moons, the surface material is a mixture of ice and silicate, where Koschny and Grün (2001a) find a prefactor of $c_1 = 6.69 \times 10^{-8}(0.015)^{x/100}$, where x is the fraction of silicate in percent (0% = pure ice, 100% = pure silicate), and exponents $c_2 = 1.08$, 1.27, and 1.27 for 5%, 10%, and 20% silicate content, respectively.

The yield is defined as the ratio of the total mass ejected by an impactor to the impactor's mass, $Y = \frac{\sum m_\mathrm{e}}{m_\mathrm{imp}}$. As the mass of the ejecta is proportional to the volume of the impact crater, the yield is therefore a function of the impactor mass, the impact speed, and the composition of the target's surface (in SI units),

$$Y = 6.69 \times 10^{-8}(0.015)^{x/100}\, \rho_t\, 2^{-b}\, m_\mathrm{imp}^{b-1}\, v_\mathrm{imp}^{2b}, \tag{4}$$

where

$$\rho_t = \left(\frac{1 - x/100}{927} + \frac{x/100}{2800} \right)^{-1} \tag{5}$$

is the mean mass density of the material at the target surface assuming a linear mixing model with mass densities $\rho_\mathrm{ice} = 927\ \mathrm{kg/m^3}$ for ice and $\rho_\mathrm{sil} = 2800\ \mathrm{kg/m^3}$ for silicate (Koschny and Grün 2001a). The yield for a pure ice target as a function of impactor radius and impact

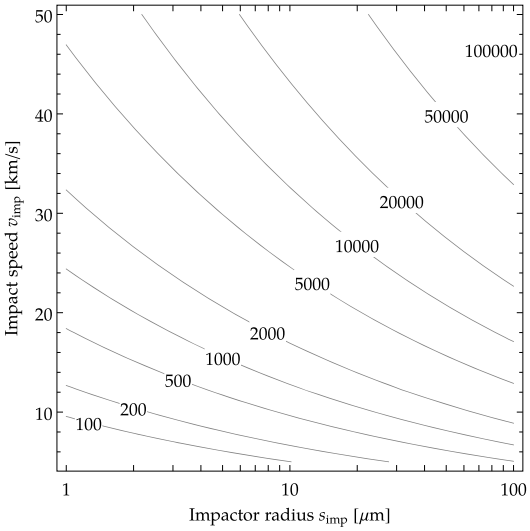

Fig. 5 Yield as a function of impactor radius and impact speed for pure ice, calculated with the empirical relation (4) from Koschny and Grün (2001a)

speed is shown in Fig. 5. For typical sizes and speeds, it varies by about three orders of magnitude. The total mass ejected from the target surface per unit time is,

$$M^+ = F_{\text{imp}} Y S, \tag{6}$$

where F_{imp} is the impactor mass flux and S is the target surface area.

The cumulative size distribution of the debris is assumed to be a power law with exponent $-q$, so that the number of particles with sizes larger than $a_{\min}$ ejected from the target surface per unit time is given by,

$$N(> a_{\min}) = \frac{3-q}{q} \frac{M^+}{m_{\max}} \left(\frac{a_{\max}}{a_{\min}} \right)^q, \tag{7}$$

where $a_{\min}$ ($m_{\min}$) and $a_{\max}$ ($m_{\max}$) are the minimal and the maximal ejecta size (mass), respectively. The index q depends on the target material and ranges from 1.5 for loose material to 3 for solid targets (Krivov and Jurewicz 1998). Buhl et al. (2014) suggest that the different impact conditions, rather than the different materials are the main reason for the various indexes. They distinguish between impacts on three different targets:

1. For a semi-infinite target, the strongly affected material is excavated and typically exhibits an index of 2.5. The weakly affected material has a smaller index and remains in the crater.
2. For a large disrupted target, the amount of strongly affected material (index 2.5) is approximately the same, but the weakly affected material (index < 2.5) is also released, which in total results in an index *smaller* than for the semi-infinite target.
3. In the case of a small disrupted target, the target volume is smaller than the volume of the strongly affected material, but the same amount of energy is released into a smaller volume, which leads to smaller fragments and an index *larger* than for the semi-infinite target.

Impact experiments with relatively small and fast projectiles (Takasawa et al. 2011), which better resemble impacts of interplanetary dust particles (micron-sized particles with speeds

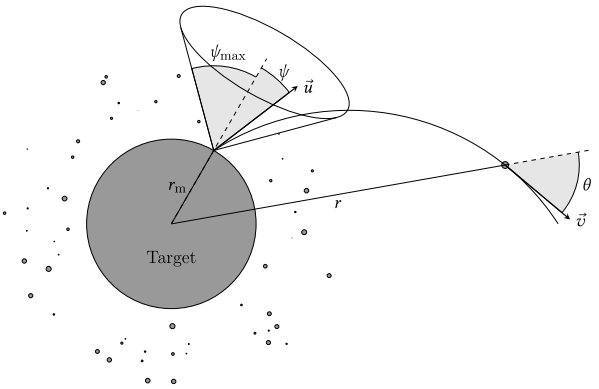

Fig. 6 Sketch of the impactor-ejecta process. A fast impactor hits a moon and releases material from its surface within a cone with a half-opening angle $\psi \in [0°, 90°]$. Individual particles are ejected at a distance $r_{\rm m}$ from the center of the moon with velocity **u** and direction ψ measured from the normal to the moon's surface at the ejection point

of a few 10 km/s), show a trend to steeper power laws. The *differential* size distribution is given by $n(a) = \frac{{\rm d}N(>a)}{{\rm d}a}$, and the distribution is normalized to the total mass ejected per unit time as,

$$\frac{4}{3}\pi\rho_t \int_0^{a_{\max}} a^3 n(a)\, {\rm d}a = M^+. \tag{8}$$

With estimates for the total mass ejected, a steady state ejecta model can be derived. To model the ejecta distribution, ejecta are started from the target, independently of the launch position, with speed u at an angle ψ measured from the normal to the surface. A typical assumption is that the fragments are ejected uniformly distributed (in terms of solid angle) in a cone of half-opening angle $\psi_{\max} \in [0°, 90°]$, with the angular distribution given by (e.g., Horányi et al. 2015),

$$f_\psi(\psi) = \frac{\sin\psi}{1 - \cos\psi_{\max}}\, \Theta(\psi_{\max} - \psi). \tag{9}$$

The impact-ejection process and relevant variables are depicted in Fig. 6. For initial conditions, it is usually assumed that the particle sizes and speeds at the moment of ejection are uncorrelated. In this case, all ejecta are launched with the same speeds regardless of their size. Impact experiments and scaling laws (Housen and Holsapple 2011) show that the *differential* speed distribution is proportional to a power law with exponent $-(\gamma + 1)$,

$$f_u(u) = \frac{\gamma}{u_{\min}^{-\gamma} - u_{\max}^{-\gamma}}\, u^{-\gamma-1}\, \Theta(u - u_{\min})\Theta(u_{\max} - u), \tag{10}$$

where $u_{\min}$ and $u_{\max}$ and the minimum and maximum velocities respectively, and $\Theta(x)$ is the unit step function, which is unity for $x \geq 0$ and zero otherwise. The index γ depends on properties of the target material and ranges from $\gamma = 1$ for (highly) porous to $\gamma = 2$ for nonporous materials (Krivov et al. 2003).

Conservation of mechanical energy requires the ejecta to have less kinetic energy than the impactor. Assuming separable size and speed distributions, the relation between Y, γ, and $u_{\min}$ reads (Krüger et al. 2000),

$$\frac{K_{\rm e}}{K_{\rm imp}} = Y\, \frac{\gamma}{2-\gamma} \left(\frac{u_{\min}}{v_{\rm imp}}\right)^2 \left[\left(\frac{u_{\min}}{u_{\max}}\right)^{\gamma-2} - 1\right] \quad \text{for } \gamma \neq 2 \tag{11}$$

or

$$\frac{K_e}{K_{imp}} = 2Y\left(\frac{u_{min}}{v_{imp}}\right)^2 \ln\left(\frac{u_{max}}{u_{min}}\right) \quad \text{for } \gamma = 2, \tag{12}$$

where the subscripts '*imp*' and '*e*' refer to impactor and ejecta related quantities, respectively. Hard surfaces (e.g. ice) are generally less dissipative than soft surfaces (e.g. snow, regolith). The minimum ejection speed is found by assuming a plausible value for the kinetic energy ratio of a few tens of percent of the kinetic energy of the impactor (Asada 1985; Hartmann 1985) and solving the above equations for u_{min}. We note the constraint of a minimum velocity is an approximation to simplify the mathematical formalism; the true velocity distribution most likely does not has an exact cutoff velocity.

Integrating Equation (10) for $u > v_{esc}$ gives the fraction of escaping ejecta ("efficiency") as,

$$F(> v_{esc}) \approx \left(\frac{u_{min}}{v_{esc}}\right)^{\gamma}, \tag{13}$$

which is a few percent for the larger moons and (close to) unity for moons smaller than about one hundred kilometers. Ascending and descending ejecta form a dust cloud around the target body. Some ejecta can escape the target's gravity, while others fall back to the surface. In (dynamical) steady state, escaping and re-impacting grains are continuously removed from the cloud and replaced at the same rate by subsequent ejecta.

5.2 Dust Clouds Around the Galilean Satellites

Dust clouds have been observed for the Galilean moons Europa (Krüger et al. 2003), Ganymede (Krüger et al. 1999), and Callisto (Krüger et al. 2003). The spacecraft Galileo arrived at Jupiter in 1995 and studied the Jovian system until 2003. Galileo performed several flybys of all four Galilean moons, with distances at closest approach between a few hundred and a few thousand kilometers. After mid-1999, the flybys were not suitable for the observation of the clouds as the orientation of the spacecraft prevented the detection of dust particles close to the moons. During many of the earlier flybys, the impact rate measured with the Dust Detector System (DDS) (Grün et al. 1992) showed a sharp peak centered around closest approach. This indicates increased concentrations of dust in the vicinity of the Galilean moons, while the symmetry of the measured profile suggests a global source.[1]

During the single suitable Io flyby only 4 dust particles were detected, but 64, 38, and 35 particles with masses larger than 10^{-16} kg (detector threshold) were detected during the 8, 4, and 3 flybys of the moons Europa, Ganymede, and Callisto, respectively. The particle size distribution can be fit by a power law with exponents $q = 1.74 \pm 0.12, 2.46 \pm 0.12$, and 2.58 ± 0.42 (Krüger et al. 2003) for ejecta from the three outer moons assuming the spacecraft velocity relative to each moon as impact speed of the dust particles. Using the speed obtained from the calibration of the dust detector, the exponents are closer together but generally smaller (1.5–1.8). These slopes are in agreement with the typical slopes expected for particles generated by the process of impact-ejection (1.5–3). The average particle radius is between 0.5 and 1 microns, which is consistent with ejecta sizes generated by impactors of 1 µm to 100 µm. This suggests that impact-ejection is the most likely source for the dust clouds around the Galilean satellites.

[1] In comparison to a local source such as cryovolcanism at the south polar terrain of Saturn's moon Enceladus (Spahn et al. 2006).

The number densities in the clouds around the moons (10^{-3} m^{-3} at $r = 0.1\,r_{\rm m}$) are up to three orders of magnitude larger than the number densities of the dust in the region between them (10^{-6} m^{-3}, see Krivov et al. 2002). The density in the clouds is dominated by bound particles as only a small fraction of the ejecta is launched with speeds larger than the high escape velocity of the Galilean satellites.

A model for a steady state dust cloud around a planetary satellite was first developed by Krüger et al. (2000) and Krivov et al. (2003). For interplanetary meteoroids at Jupiter, we use (Krivov et al. 2003)

$$F_{\rm imp}^{\infty} = 7.6 \times 10^{-16}\ \mathrm{kg/(m^2\,s)} \tag{14}$$

$$v_{\rm imp}^{\infty} = 9\ \mathrm{km/s}, \tag{15}$$

and we modify these values for the effect of gravitational focusing as previously described. We note the impactors will arrive with a speed distribution, rather than a single velocity, and utilize this delta function velocity distribution for mathematical simplicity. Because impact-ejecta from the Galilean moons are the most likely source for dust detected between their orbits (Krivov et al. 2002), we assume an upper speed limit larger than the escape velocity of these bodies ($u_{\rm max} > 3$ km/s). This estimate possibly ignores a very small fraction of high-speed ejecta, but the results depend only weakly on $u_{\rm max}$ owing to the steepness of the speed distribution.

For the case of a moving target—where the spherical symmetry is broken—Sremčević et al. (2003) developed an asymmetric model. In these models, it is assumed (for simplicity and according to the current impact-ejection model) that the distribution of the particle sizes and their speeds at the moment of ejection is uncorrelated. The distribution obeys phase space conservation, with the dynamics in the vicinity of the parent body (to a good approximation) governed by the two-body problem. Krivov et al. (2003) give for the number density of bound ejecta at a distance r (in units of the satellite radius $r_{\rm m}$) from the center of the body,

$$n_{\rm bound}(\tilde{r}) = \frac{N^{+}}{2\pi r_{\rm m}^2 v_{\rm esc}}\,\gamma \tilde{u}_{\rm min}^{\gamma}\,\tilde{r}^{-2.5} K_{\rm bound}(\tilde{r}), \tag{16}$$

and for unbound ejecta,

$$n_{\rm unbound}(\tilde{r}) = \frac{N^{+}}{4\pi r_{\rm m}^2 v_{\rm esc}}\,\gamma \tilde{u}_{\rm min}^{\gamma} c_0(\gamma)\,\tilde{r}^{-2} K_{\rm unbound}(\tilde{r}), \tag{17}$$

where the tilde denotes normalized variables, $\tilde{r} = r/r_{\rm m}$ and $\tilde{u}_{\rm min} = u_{\rm min}/v_{\rm esc}$. $K_{\rm bound}(\tilde{r})$ and $K_{\rm unbound}(\tilde{r})$ are form factors only weakly depending on distance and tending to unity far from the moon. $c_0(\gamma) = \frac{\sqrt{\pi}\,\Gamma((\gamma+1)/2)}{\gamma\,\Gamma(\gamma/2)}$ is a monotonically decreasing function with relevant values between $c_0(1) = 1$ and $c_0(2) = \frac{\pi}{4} \approx 0.79$. $\Gamma(x+1) = x \cdot \Gamma(x)$ with $\Gamma(1) = 1$ is the Gamma function. The dust densities decrease with increasing height above the moon's surface, with $r^{-2.5}$ and r^{-2} for large $\tilde{r}$ and particles in bound and unbound orbits, respectively. Figure 7 shows the observed dust densities for the dust cloud around the moon Ganymede and the calculated dust densities predicted by the model from Krivov et al. (2003).

Given estimates for the bound and unbound densities of the ejecta clouds, the total content of the bound exosphere and loss rate can be calculated. For the surface properties of the moons, we adopt numbers from Showman and Malhotra (1999). For bright Europa, we use pure ice ($x = 0\%$); for the volcanically active moon Io, we use pure silicate ($x = 100\%$);

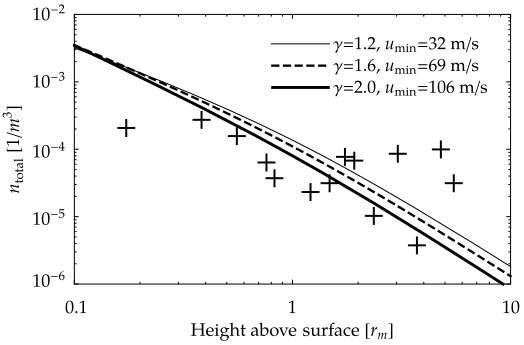

Fig. 7 Number density ejecta at a distance r (in $r_m = 2634$ km) from the surface of Ganymede. The crosses are dust densities obtained by Krüger et al. (2000) from *in situ* measurements of the Galileo DDS during flybys of Ganymede. The solid lines are number densities calculated using the model from Krivov et al. (2003) with $Y = 1000$, $\alpha = 2.5$, $m_{min} = 10^{-16}$ kg, and $m_{max} = 10^{-8}$ kg, and for three different sets of parameters for the speed distribution

and for Ganymede and Callisto intermediate values are used, $x = 70\%$ and $x = 30\%$ respectively. With this and assuming an impactor population dominated by 100 µm-sized projectiles (Divine 1993), we find a yield of $Y \approx 1000, 20000, 1000$, and 2000 for the respective moons. As a result, the estimated amount of material ejected from each moon is in the order of 10–100 kg/s. The lifetime of the particles depends on the parameters of the ejecta speed distribution. It is dominated by the large number of slow ejecta but only weakly depends on the maximal ejection speed. For the Galilean satellites, the average lifetime is between several tens of seconds and a few hundred seconds. Then the mass of the dust in a steady state cloud is on the order of 10^3–10^4 kg. Due to the large escape velocity of the moons, the fraction of escaping ejecta is relatively small (on the order of 0.1–1%). As a result, the estimated amount of material ejected from each moon into circumplanetary space is between 0.01 kg/s and 1 kg/s. Escaping ejecta form a tenuous ring across the orbits of the Galilean moons (Krivov et al. 2002).

In the current impact-ejection model, it is assumed that the particle sizes and speeds at the moment of ejection are uncorrelated. In contrast, at least for bigger particles theoretical modeling (Melosh 1984) and impact experiments (Nakamura et al. 1994; Onose and Fujiwara 2004) suggest that larger fragments are on average launched with lower speeds. Sachse et al. (2015) have dropped the assumption that the ejecta sizes and ejection speeds are uncorrelated and applied the new model to dust clouds around planetary satellites. They find that both models can fit *in situ* measurements of the total density equally well, but differences are visible for micron-sized particles or larger. However, the exact form of the correlation is poorly constrained as there is only a small number of studies focusing on this aspect of the impact-ejection process. A further refinement requires additional impact experiments, namely with projectile sizes and impact speeds similar to micron-sized interplanetary impactors.

5.3 The Lunar Dust Cloud

While an ejecta cloud surrounding the Moon was expected from observations of the Galilean satellites, until recently, it had not been explored. The Lunar Atmosphere and Dust Environment Explorer (LADEE) mission orbited the Moon from October 2013 to April 2014, with

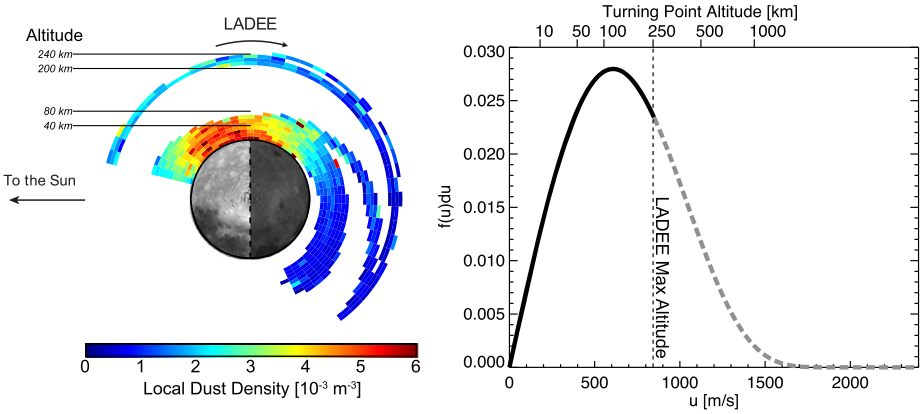

Fig. 8 *Left.* The dust density distribution about the Moon, calculated using $\sim$ 140,000 impacts averaged over LADEE's 6 months of operations in lunar orbit. White regions indicate locations either LADEE did not visit or that LDEX could not take measurements due to sun pointing constraints. Altitude bands are not to scale. *Right.* The inferred surface ejecta velocity distribution from the altitude density fit. The dotted line indicates the maximum altitude explored by LADEE, above which the distribution function is an extrapolation

a primary science objective to characterize the neutral and dust environment of the Moon (Elphic et al. 2014). Onboard, it carried the Lunar Dust Experiment (LDEX), an impact ionization dust detector capable of individually detecting impacts from grains with radii $a \geq 0.3$ µm (Horányi et al. 2014). LDEX discovered a permanently present, asymmetric lunar dust cloud (Horányi et al. 2015). It detected $\sim$ 140,000 individual dust impacts during its six months of observations with $\sim$ 2,000 orbits. The observed dust cloud was found to be most dense on the apex hemisphere (in the direction of orbital motion of the Earth-Moon system about the Sun), with a slight cant towards the Sun, and is generated by the continual bombardment of meteoroids to the lunar surface (Fig. 8).

As described in further detail in the Meteoroids review paper, the distribution of meteoroids impacting the Earth-Moon system is typically divided into two categories, meteoroid showers and the sporadic background. Meteoroid showers are periods where highly collimated beams of particles impact a body from a narrow region in the sky known as the radiant. The sporadic background is larger in overall flux than the total contribution from meteoroid showers and is further broken up into distinct sources. In the ecliptic plane, these sources are the Helion (HE), Apex (AP), and Anti-Helion (AH) (Jones and Brown 1993), with an additional weak Anti-Apex (AA) source (Janches et al. 2000).

The lunar dust density distribution in the equatorial plane was found to be primarily generated by the HE, AP, and AH sporadic sources (Szalay and Horányi 2015a), with a minor contribution potentially coming from the AA source (Szalay and Horányi 2016b). As the Moon orbits the Earth with a relative velocity of 1 km/s, it is continually moving into and away from these sporadic meteoroid sources at different lunar phases. Due to this relative motion, the lunar dust cloud was found to wax and wane on the lunar synodic period (Szalay and Horányi 2015a). Further analyses of the ejecta cloud structure incorporating a dynamical meteoroid model enabled estimations of the relative quantities of short-period and long-period comets impacting the lunar surface (Janches et al. 2018). During several of the known meteoroid showers, such as the Geminids and Quadrantids, LDEX observed temporary enhancements of the lunar dust cloud, localized on the hemisphere exposed to the incident meteoroid shower flux (Szalay and Horányi 2016a; Szalay et al. 2018). Most

notably during these periods, LDEX intermittently observed "bursts" of particles, which are interpreted as direct measurements of transits through dense ejecta plumes.

Unlike at the Galilean moons, an exponential fit was found to be in good agreement with the altitude distribution, with the form $n(h) = n_0 e^{-h/h_0}$, where h is the altitude in km above the lunar surface, n_0 is the density at $h = 0$, and $h_0 = 200$ km is the scale height (Szalay and Horányi 2016b). The cumulative size index of lunar impact ejecta was found to be $q = 2.7$ and did not vary significantly with time or altitude (Horányi et al. 2015). Factoring the altitude, size, and local time dependencies, the average lunar dust density in the equatorial was found to be well represented by,

$$n(h, \varphi, a) = e^{-h/h_0} a_\mu^{-q} n_w \sum_s w_s \cos^3(\varphi - \varphi_s) \Theta\big(|\varphi - \varphi_s| - \pi/2\big), \tag{18}$$

where a_μ is the particle radius in μm, s represents each ecliptic sporadic source, Θ is the Heaviside function, φ_s is the characteristic angle for each of the four source radiants (65°, 0°, −65°, 180°) (Campbell-Brown 2008), $n_w = 3.3 \times 10^{-4}$ m^{-3}, and w_s is the relative weight (0.24, 0.49, 0.24, 0.03) for the HE, AP, AH, & AA sources respectively. The relative ratios of AP to HE/AH sources were taken from a combination of Earth-based radar measurements (Campbell-Brown 2008) and lunar dust measurements (Szalay and Horányi 2016b). These ratios may vary throughout the year, following any relative variations in their respective sources; the values quoted here give an average case for the lunar dust cloud.

The dust density altitude distribution can be inverted to determine the initial velocity distribution function for dust grains ejected from the lunar surface,

$$f(\tilde{u}) = \frac{\eta \tilde{u}}{(1 - \tilde{u}^2)^2} e^{-\frac{\beta \tilde{u}^2}{1 - \tilde{u}^2}} \tag{19}$$

where $\tilde{u} = u/u_m$ with $u_m = 2.4$ km/s (lunar escape speed), $\beta = 8.69$, and $\eta = 7.2 \times 10^{-3}$ s/m (Szalay and Horányi 2016b), shown in Fig. 8. This distribution was derived assuming LDEX only detected bound grains at their turning points; it therefore represents an approximation of $f(\tilde{u})$ at the Moon.

There is an apparent discrepancy between this velocity distribution and the power law consistent with the ejecta clouds of the Galilean moons. However, Galileo and LADEE visited a different range of altitudes above their respective airless bodies. LADEE visited a range of a few to ∼ 250 km in altitude such that it observed the ejecta cloud up to $\tilde{r} = 0.14$. The inferred velocity distribution monotonically increases for the majority of the altitude range covered by LADEE, with a peak at ∼ 600 m/s (corresponding to a turning point altitude of ∼ 120 km). In the velocity range from 600 m/s to 840 m/s, the lunar velocity distribution monotonically decreases, however, only a small portion of the descending portion of this distribution is sampled. In comparison, the Galileo DDS detected 141 impacts throughout its 16 flybys of the Galilean moons at distances of $\tilde{r}$ in the range of 0.13 to 8 (Krüger et al. 2003), with about half of the flybys above $\tilde{r} = 2$. Therefore, the two missions probed different ejecta cloud regions and we can only infer information about the velocity distribution relative to the applicable initial velocities required to reach these given altitudes. It is possible that the lunar ejecta velocity distribution trends toward a power law for large velocities and that LADEE simply did not visit high enough altitudes to address this issue. Additionally, as previously discussed, the surface ejection properties and subsequent velocity distributions between the icy Galilean moons and the silicate regolith dominated lunar surface are most likely to be characteristically different. Lastly, relaxing the assumption of a single typical impactor/ejecta plume and allowing the speed and mass distributions to be correlated (Sachse et al. 2015) may aid in understanding the impact ejecta measurements discussed here.

5.4 Bound Ejecta Clouds Around Other Airless Bodies

In addition to the observed ejecta clouds at the Galilean satellites and the Moon, impact ejecta should be generated at airless bodies throughout the solar system. Mercury likely possesses a relatively dense impact ejecta cloud from meteoroid bombardment, given its similarity to the Moon and the increased meteoroid flux deeper in the heliosphere (e.g., Hahn et al. 2002; Pokorný et al. 2017). The overall magnitude of the meteoroid flux at Mercury is still fairly uncertain (e.g., Cintala 1992; Borin et al. 2009, 2016); however, future in-situ measurements by the Mercury Dust Monitor on-board the BepiColombo spacecraft (to be launched to Mercury in late-2018) may reveal the presence of an impact ejecta exosphere at Mercury (Nogami et al. 2010).

Similar to the Galilean satellites, one also expects impact ejecta clouds at the major saturnian satellites such as Iapetus, Rhea, Dione, Tethys, Enceladus, and Mimas. To date, however, no such positive detection has occurred, with the exception of the massive Phoebe ring (Verbiscer et al. 2009). Perhaps the biggest obstacle to detection of impact ejecta clouds at the saturnian satellites is the presence of the large and dusty E-ring generated from the Enceladus plumes. Analysis of Cassini dust impact rate observations during fly-bys of Enceladus have fit both plume ejecta and impactor ejecta to the total flux measurements (Spahn et al. 2006a; Kempf 2008); however, the resulting impact ejecta contributions are typically small with respect to the plume measurements. Thus, no clear evidence has been found for clouds around the E ring moons of Saturn,[2] which suggests that the ejecta cloud dust densities are lower than previously predicted by extrapolation of results at the Galilean satellites. Possible reasons for this may be a lower impactor flux (e.g., Poppe 2016), impactor size and/or impact speed, and/or a more dissipative surface, possibly due to a layer of icy E ring particles ('snow') soaking up more of the impactor's kinetic energy.

Smaller bodies in the solar system will also generate ejecta in their near vicinity, however, much of this ejecta will be unbound (e.g., Szalay and Horányi 2016c). The main factor that determines the total ratio of bound to unbound ejecta is the mass of the body, however, the speed distribution also plays an important role. Assuming the speed distribution of ejecta is the same as that of the Moon and a mass density of 3 g/cc for airless bodies, an airless body would need to be larger than 500 km to retain at least 50% of its impact ejecta. Hence, and as discussed in Sect. 6.2.1, most small bodies near 1 AU shed the large majority of their impact ejecta and therefore the bound component of ejecta at smaller bodies is particularly tenuous.

6 Airless Bodies as Sources of Dust

6.1 Phobos and Deimos

Mars' moons Phobos and Deimos have long been suspected to be parents of a pair of tenuous dust tori encircling Mars due to escaping impact ejecta (Soter 1971). The Russian PHOBOS-2 mission observed unusual variations in the interplanetary magnetic field near the location

[2] Rhea and the E ring moons in general are currently debated for having or not having dust clouds that can be measured against the relatively strong E ring background (Spahn et al. 2006a), which is supplied by cryovolcanism on Enceladus (Schmidt et al. 2008). Two *in situ* measurements have been conducted so far by the spacecraft Cassini. The first one is inconclusive as it depends on a single data point, the second one does show a profile but the measured peak is much wider than predicted by the model from Krivov et al. (2003).

of Phobos' orbit, which were at the time interpreted as evidence of solar wind mass loading by either a neutral gas or dust torus (Dubinin et al. 1990, 1991; Sauer et al. 1993; Barabash and Lundin 1994). This suggestion gave rise to a prolific series of investigations into the underlying theoretical physics of the martian dust tori by a number of authors (e.g. Ip and Banaszkiewicz 1990; Horányi et al. 1990, 1991; Tátrallyay et al. 1992; Kholshevnikov et al. 1993; Krivov 1994; Juhász et al. 1993; Juhász and Horányi 1995; Ishimoto 1996; Krivov and Hamilton 1997; Makuch et al. 2005). The underlying prediction from these models is a pair of dust tori around Mars: one from Phobos ejecta that is strongly confined to Phobos' orbital plane and one from Deimos ejecta that is more diffuse and inclined. Despite this wealth of modeling, no observational signatures, either from in-situ or remote sensing observations, have detected the presence of these putative dust rings (Showalter et al. 2006; Krivov et al. 2006; Øieroset et al. 2010). These attempted measurements have placed fairly stringent upper limits to the Phobos and Deimos tori, with maximum normal optical depths of $\approx 3 \times 10^{-8}$ and 10^{-7}, respectively. In-situ measurements by impact ionization dust detectors may be required for a final determination as to the presence and density of these tori.

6.2 Asteroids

In the discussion below, we focus on dust phenomena relating to asteroids (some of which have cometary-like activity), leaving the cometary discussions for the Comets review paper in this Topical Collection.

6.2.1 Impact-Ejecta Production Rates in the Asteroid Belt

Ejecta clouds for Near Earth Asteroids (NEAs) have been predicted based on lunar measurements (Szalay and Horányi 2016c), and the spatial distribution of ejecta dust around Main Belt asteroids is expected to be qualitatively similar to that around NEAs. Asteroidal ejecta clouds are predicted to be predominantly unbound given the relatively low asteroidal gravity. For example, a 10 km radius asteroid near 1 AU is predicted to lose $> 99.9\%$ of the ejecta generated by meteoroid bombardment. A quantitative assessment requires knowledge of the meteoroid flux in the asteroid belt, such as predicted by ESA's IMEM model (Dikarev et al. 2005) and the surface response to such fluxes. The spatial density of meteoroids in the asteroid belt is likely one order of magnitude lower than at 1 AU (Landgraf et al. 2002), suggesting lower unbound ejecta densities around asteroids in this region compared to NEAs. Despite these lower production rates for any individual asteroid, Main Belt asteroids steadily produce ejecta that contribute to supplying the interplanetary dust complex, although at a share of $< 10\%$ (Nesvorný et al. 2010).

Collisions with larger asteroids are less frequent with increasing impactor size but produce large amounts of dust that can be observed with Earth-based telescopes. The typical relative velocity between Main Belt asteroids is 5.3 $\mathrm{km\,s^{-1}}$ (Bottke et al. 1994), and the mass of particles ejected faster than the impacted body's escape speed is comparable to the mass of the projectile (Housen and Holsapple 2011; Jewitt et al. 2011). The most direct observation of an impact on a Main Belt asteroid is that of a decameter-sized projectile onto 57 km-diameter asteroid (596) Scheila (Jewitt et al. 2011; Bodewits et al. 2011; Ishiguro et al. 2011a,b). The impact excavated a dust cloud of 0.1–100 µm-sized grains having a total mass of $\sim 10^8$ kg. The dust was dispersed by radiation pressure within ~ 2 months. Impacts onto smaller asteroids are likely to eject larger debris due to the lower escape speed.

The frequency of collisions between Main Belt asteroids is uncertain. Collisional models suggest a rate of one catastrophic collision per year for 100-m-sized objects, with subcatastrophic impacts being more frequent (Bottke et al. 2005). Denneau et al. (2015) instead

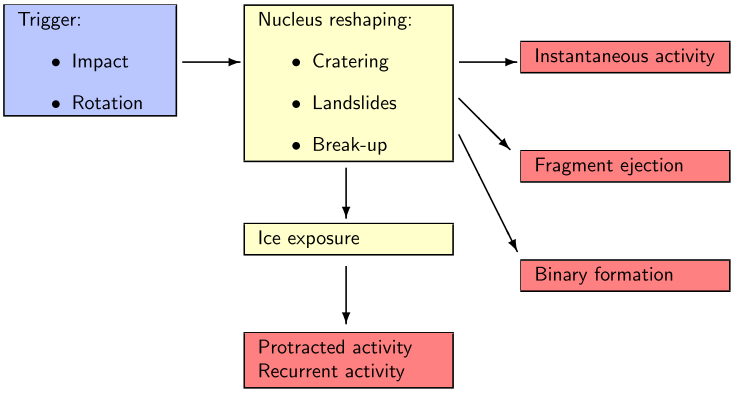

Fig. 9 An overview of the processes involved in the activation of asteroids

find that a rate of one catastrophic collision per year is consistent with Pan-STARRS detection rates only for 7 m-sized objects, while encounters of 100 m-sized objects would be less frequent. Bodewits et al. (2014) interpret a change in Scheila's rotational lightcurve as the signature of surface alteration due to the impact. They find that the < 100 m impactor affected the albedo of an area of 3.5–10 m in radius, likely by covering it in a thin (2 mm–2 cm) ejecta blanket of bright material.

Assuming that at least two out of the 17 active asteroids listed in Table 1 were impact-triggered (176P and Scheila, because their slow rotation rates exclude rotational disruption), we expect that at least 10% of the active asteroids are impact-triggered. Combining this with the estimated total number of active asteroids of 100 (Sheppard and Trujillo 2015) and assuming that the generated dust remains visible for $\sim 10\%$ of an orbital period, we obtain a (telescopically detectable) impact rate of one per year and an impact-generated dust production of order 10^8 kg per year, within an uncertainty of at least one order of magnitude.

6.2.2 Active Asteroids

The emission of dust from asteroids has been detected by telescopic observations in ~ 20 objects (Hsieh and Jewitt 2006; Jewitt 2012; Jewitt et al. 2015d). These active asteroids temporarily display comet-like comae and tails, but have asteroidal orbits with $T_J > 3$ (Kresak 1982; Kosai 1992). Figure 9 summarizes many of the processes occurring on these airless bodies, as described below.

A prime tool to understand the processes effectuating the dust emission is the analysis of the dust tail morphology and temporal evolution through model calculations of the dust dynamics under the influence of initial velocity, solar radiation pressure, and gravity (Finson and Probstein 1968; Agarwal et al. 2010; Fulle et al. 2010; Moreno et al. 2017). The activity shows strong variation between objects, probably reflecting the diversity of underlying processes. In general, asteroid activity seems to be triggered by some violent process of very short duration, such as an impact or re-shaping due to centrifugal forces, where both processes are likely to have been observed in different objects. This trigger process is accompanied by the ejection of dust, debris, and sometimes larger fragments visible to telescopes. In addition, it can lead to the catastrophic breakup of the object or the formation of a binary system. In some active asteroids, such a trigger process has apparently uncovered ice previously hidden in the interior of the asteroid. Exposed to enhanced solar irradiation

around perihelion, the ice sublimates and carries along dust, leading to comet-like activity in the classical sense.

At least one of the active asteroids, (596) Scheila, has been impacted by a second, smaller asteroid (Jewitt et al. 2011; Bodewits et al. 2011; Moreno et al. 2011b). The ejected dust formed an impact cone and a downrange plume, and was subsequently driven away from the nucleus by solar radiation pressure (Ishiguro et al. 2011a,b). Due to Scheila's comparatively large size (113 km diameter), only small dust grains could escape from the nucleus' gravity field, which were subsequently dispersed by radiation pressure within approximately one month.

The rotation period of a small asteroid of irregular shape or albedo can be changed by a torque from the asymmetric emission of thermal radiation (so called YORP-effect) (Rubincam 2000) or by localised outgassing. If the centrifugal force compensates gravity at the equatorial surface, the body will shed material from its surface or even breakup entirely (Hirabayashi and Scheeres 2013; Veras et al. 2014; Pravec et al. 2010), depending on its shape and composition (Hirabayashi 2015). The critical rotation rate at which a body will disintegrate depends on its bulk density and cohesion. The lack of observations of asteroids > 100 m in diameter rotating at periods < 2.2 h (Warner et al. 2009) is interpreted as evidence that these bodies are nearly-strengthless rubble piles bound only by gravity, while smaller asteroids seem to have a considerably higher internal strength. The 2.2 h spin barrier seems to reflect rotational disruption as an effective process of asteroid disintegration or re-shaping.

Several active asteroids are suspected to have undergone rotational mass shedding or disintegration. The evidence is mainly indirect, based on the exclusion of alternatives such as impact or sublimation (311P: Jewitt et al. 2013, 2015a; Hainaut et al. 2014; Moreno et al. 2014, P/2013 R3: Jewitt et al. 2014a), near-critical rotation periods (331P: Drahus et al. 2015, 133P: Hsieh et al. 2004, (62412): Sheppard and Trujillo 2015), large fragments (P/2010 A2: Jewitt et al. 2010, 331P: Drahus et al. 2015), ejection speeds comparable to the gravitational escape speed (133P: Jewitt et al. 2014b, 288P: Agarwal et al. 2015, P/2010 A2: Jewitt et al. 2010, P/2013 R3: Jewitt et al. 2014a), and in one case planar ejection velocities (P/2010 A2: Agarwal et al. 2013). In some of these objects (133P, 288P), the fast rotation seems to support gas drag in lifting dust, while in others it only triggered instantaneous (P/2010 A2, 331P) or repeated (311P) mass shedding without uncovering ice, or a catastrophic disruption (P/2013 R3). A detailed discussion of individual objects is given in Jewitt et al. (2015d).

Currently nine known asteroids have shown activity for an extended period of several months around perihelion, and for at least five of these the activity recurred in subsequent perihelion passages (133P, 238P, 288P, 313P, 324P), while the remaining four had at the time of writing not been observed during a second perihelion passage (P/2012 T1, P/2015 X6, 259P, P/2016 J1). Protracted and recurrent activity are taken as strong indicators for dust ejection by a flow of sublimating gas, as this is the only known process modulated by the heliocentric distance that is able to lift dust of the observed quantity and size over an extended period of time in the Main Belt (Jewitt 2012). Thermal models of asteroid interiors have shown that the conservation of primordial water ice in the interiors of Main Belt asteroids is possible, while more volatile species are likely depleted (Schorghofer 2008, 2016; Prialnik and Rosenberg 2009; Snodgrass et al. 2017). The gas production rates required to lift the observed amount of dust are below the detection limit of currently available instruments, such that the non-detection of water vapor around active asteroids is not a proof against its presence. Sublimation-driven dust activity is discussed in more detail in the Comets review paper.

Dust can also be accelerated above an asteroid's escape speed by thermal fracturing and dehydration at temperatures exceeding $\sim$ 1000 K (Jewitt 2012). While this process is unlikely to play a significant role in the Main Belt, it is probably responsible for the recurrent ejection of micron-sized dust from asteroid (3200) Phaethon during its 0.14 AU perihelion passage (Jewitt and Li 2010; Li and Jewitt 2013; Jewitt et al. 2013b; Hui and Jewitt 2017). (3200) Phaethon has been suggested to be the parent body of the Geminids stream.

No direct measurements exist concerning the bulk density, porosity, composition, or optical properties of dust from active asteroids. Assuming a size-independent albedo and density, dust ejection models are usually consistent with power-law cumulative size distributions having exponents between -2.0 and -2.7. Jewitt et al. (2015a) found a size distribution steepening towards smaller sizes in 311P. Maximum particle sizes found in sublimation-driven asteroids are below 1 cm, while dust ejected from asteroids suspected to have been impacted or rotationally disrupted reaches up to 1 m in size. P/2010 A2 and 331P displayed a debris trail of decimeter- to meter-sized chunks at least several years after the dust-producing events (Jewitt et al. 2013a; Drahus et al. 2015). In four active asteroids, the dust terminal speeds have been found to be less than the gravitational escape speed from the nucleus. At least two of these are fast rotators, such that it is suspected that in these objects the escape of dust is facilitated by the centrifugal force, the dust leaves the nucleus at a speed comparable to the escape speed and decelerates with increasing nucleus distance. In most other active asteroids, inferred dust speeds range between 1 and 10 m/s. No obvious correlation has been found between the nucleus size and the sizes of ejected dust.

The typical dust mass ejected from an active asteroid per orbit is of order 10^7 kg, with a variation by a factor 100 between individual objects. This is approximately a factor of 1000 less than in comets. Assuming a total number of 100 currently active asteroids (Sheppard and Trujillo 2015) and a typical orbital period of 5 years, this corresponds to a dust production rate of 6 kg s^{-1}, only 0.006–0.06% of the rate of 10^4–10^5 kg/s required to sustain the zodiacal cloud (Nesvorný et al. 2011a). It is therefore likely that active asteroids contribute only a minor fraction to the interplanetary dust complex.

As discussed in the Meteoroids review paper, the Geminid meteor stream is associated with the orbit of asteroid (3200) Phaethon (Whipple 1983), but the current level of activity of Phaethon (Jewitt et al. 2013b) is not sufficient to explain the particle sizes in the meteor stream. It is therefore likely that Phaethon lost a large amount of large debris in the past within a relatively short period of time (Ryabova 2017). Several other meteor streams in asteroidal orbits may exist (Jenniskens 2015), but their parent bodies are unknown. The detection of debris trails following active asteroids P/2010 A2 and 311P indicates that processes underlying asteroid activity can lead to the formation of a meteor stream that would be detectable as a meteor shower if the object were on an Earth-crossing orbit.

6.3 Minor Planetary Satellites

While discussed in more detail in the Rings review paper, the minor moons of the outer satellites are also known to be prodigious sources of dust grains. The tenuous, dusty rings of Jupiter are formed from ejecta produced from meteoroid bombardment of four small Jovian moons, Metis, Adrastea, Amalthea, and Thebe, and consist of three parts: the main ring, the halo, and the outer gossamer rings (e.g., Smith et al. 1979a,b). Grains ejected from these bodies undergo orbital decay from Poynting-Robertson drag and perturbations from electromagnetic interactions (Burns et al. 1999; Hamilton and Krüger 2008).

At Saturn, several of the minor moons in the inner system, including Methone, Anthe, and Pallene, have been associated with either complete rings or "arcs" of dust grains that are

Table 1 Properties of ejected dust for 17 active asteroids. Types: c: continuous, r: recurrent, i: instantaneous, e: episodic activity, f: fragments, t: debris trail, m: multiple nucleus; $v_{\rm esc}$: nucleus escape speed; $R_{\rm rot}$: nucleus rotation period; β: ratio of radiation pressure and solar gravity, related to dust radius s by $\beta = 5.77 \times 10^{-4} Q_{pr}/\rho/s$, and $Q_{pr} \sim 1$; $M_{\rm dust}$: dust mass produced per orbit; $v_{\rm dust}$: dust terminal velocities; q: exponent of power-law cumulative size distribution. References: [a] Moreno et al. (2013); [b] Agarwal and Mommert (2017); [c] Moreno et al. (2016a); [d] Hui et al. (2017); [e] Moreno et al. (2017); [f] Sheppard and Trujillo (2015); [g] Jewitt et al. (2009); [h] MacLennan and Hsieh (2012); [i] Hsieh et al. (2004); [j] Hsieh et al. (2010); [k] Jewitt et al. (2014b); [l] Hsieh et al. (2008); [m] Agarwal et al. (2015); [n] Licandro et al. (2013); [o] Agarwal et al. (2017); [p] Jewitt et al. (2015b); [q] Jewitt et al. (2015c); [r] Hsieh et al. (2015); [s] Pozuelos et al. (2015); [t] Moreno et al. (2011a); [u] Moreno et al. (2012); [v] Drahus et al. (2015); [w] Moreno et al. (2014); [x] Jewitt et al. (2015a); [y] Jewitt et al. (2014a); [z] Jewitt et al. (2010); [aa] Snodgrass et al. (2010); [ab] Hainaut et al. (2012); [ac] Jewitt et al. (2013a); [ad] Agarwal et al. (2013); [ae] Kim et al. (2017b); [af] Kim et al. (2017a); [ag] Moreno et al. (2016b); [ah] Hsieh et al. (2011); [ai] Bodewits et al. (2011); [aj] Jewitt et al. (2011); [ak] Ishiguro et al. (2011b); [al] Ishiguro et al. (2011a); [am] Moreno et al. (2011b)

Object	Type	$v_{\rm esc}$ [m/s]	$P_{\rm rot}$ [h]	β	$M_{\rm dust}$ [kg]	$v_{\rm dust}$ [m/s]	$-q$
358P[a]	c	0.2[b]		10^{-4}–0.2	1.5×10^7	0.3–12.2	−2.5
P/2015 X6[c]	c			6×10^{-5}–0.6	7×10^6	0.3–10	−2.3
P/2016 J1[d,e]	c, m	0.5			1.4×10^7	0.5–0.9	
(62412)[f]		3.9	3.33				
259P[g,h]	c	0.1			1.8×10^4	1–10	
133P[i,j,k]	c, r	1.8	3.47	6×10^{-5}–3×10^{-3}	1.8×10^7	0.02–0.13	−2.5– − 2.25
238P[l]	c, r	0.3		10^{-4}–0.1	10^5	0.2–3	
288P[m]	c, r, m[n]	0.7		0.001–0.025	9×10^6	0.06–0.3	−2.1[o]
313P[p,q,r,s]	c, r	0.5		0.01– > 0.03	10^7	0.4–2.5	−2.1– − 2.5
324P[t]	c, r	0.4		0.005–0.02	1.3×10^6	0.2–9.1	−2.5
331P[u]	i, f, t	0.7[v]	3.24	–0.03	10^8	0.5–0.7	−2.7
311P[w,x]	e	0.2		2×10^{-5}–0.6	10^7	0.02–0.07	−2.5
P/2013 R3[y]	m	0.2		$< 3 \times 10^{-5}$	2×10^{10}	0.3	
354P[z,aa,ab,ac,ad,ae,af]	i, f, t	0.04	11.36	10^{-6}–2×10^{-3}	5×10^8	0.02–0.3	−2.6– − 2.1
P/2016 G1[ag]	i	0.03			1.7×10^7	0.015–0.14	−2.0
176P[ah]	c	1.5	22.22	9×10^{-2}–0.1	7×10^4	11.2–11.8	−2.5
(596) Scheila[ai,aj,ak,aj,ak]	i	75	15.85	2×10^{-5}–0.2	6×10^8	50–100	−2.5– − 2.0

presumably being actively shed via meteoroid bombardment (Hedman et al. 2009; Sun et al. 2017). In the outer saturnian system, the massive Phoebe ring is produced via meteoroid bombardment (Verbiscer et al. 2009; Hamilton et al. 2015) and it is suspected that Saturn's other irregular satellites may also contribute to dust in the saturnian system (Tamayo et al. 2011). Uranus plays host to a complex and potentially unstable set of moon-ring systems (Smith et al. 1986; Showalter et al. 2006; de Pater et al. 2006a,b; Sfair and Winter 2009), such as the μ and ν rings associated with the moons Mab, Puck, Rosalind, and Portia.

6.4 Dust Production from Edgeworth-Kuiper Belt Objects

Edgeworth-Kuiper Belt objects (EKBOs) also may play host to dusty exospheric ejecta clouds or tori. The Pluto-Charon system has been most studied in this regards from both observational and theoretical standpoints. An early simulation by Thiessenhusen et al. (2002) predicted a dust cloud from Pluto and Charon while later investigations focused on dust torus generation by Nix and Hydra (e.g., Poppe and Horányi 2011), two of Pluto's small moons discovered in 2005 (Weaver et al. 2006). Qualitatively similar to the proposed dust torus at Mars from Phobos and Deimos, the Nix and Hydra dust tori at Pluto are believed to be generated from impact ejecta from meteoroid bombardment which are subsequently still bound in orbit around the Pluto-Charon barycenter (Poppe and Horányi 2011; Pires dos Santos et al. 2013). Pluto's two other small moons, Styx and Kerberos, may also contribute significantly to the torus density given their negligible surface gravity. To date, however, neither remote sensing observations (Steffl and Stern 2007; Throop et al. 2015) nor in-situ measurements by the New Horizons spacecraft (Bagenal et al. 2016) have detected any positive evidence of the theorized dust torus. Other EKBOs, especially those in binary or multiple systems (e.g., Noll et al. 2008; Benecchi et al. 2010), may also maintain tenuous dust exospheres and/or tori.

Despite the lack of direct observations of dust production in the Pluto-Charon system, Edgeworth-Kuiper Belt objects are a significant source of interplanetary dust grains in the solar system. Three potential production mechanisms for interplanetary dust from EKBOs have been discussed: (i) mutual collisions and grinding (e.g., Stern 1995, 1996; Stern and Colwell 1997; Davis and Farinella 1997; Durda and Stern 2000), (ii) bombardment of EKBOs from interstellar dust grains (Yamamoto and Mukai 1998), and (iii) bombardment of EKBOs by interplanetary dust grains (Poppe 2015).

Collisional evolution is thought to be an important and on-going process in the EKB, despite the relatively slow velocities compared to the asteroidal main belt. Stern (1996) calculated that collisions produce a cumulative 9.5×10^8 to 3.2×10^{11} g s^{-1} of debris over sizes ranging from submicron-sized dust to 10 km sized blocks. Assuming a collisional power-law size distribution of $a^{-3.5}$, this yields a mass production rate of 8.6×10^4–2.9×10^7 g s^{-1} for grains between 0.1 and 10 µm.

Interstellar grains flow through the entire heliosphere (e.g., Grün et al. 1994; Krüger et al. 2007; Krüger and Grün 2009; Sterken et al. 2012) and may also be a significant source of ejecta from EKBOs, based on calculations by Yamamoto and Mukai (1998), which yielded 0.1–10 µm production rates in the EKB of 3.7×10^5–2.4×10^6 g s^{-1}, similar to that estimated for mutual collisions.

Finally, bombardment of EKBOs by interplanetary dust grains may also be a contributor to the total production rate as suggested by Poppe (2015). This process is somewhat reminiscent of the "self-sustained" production models for the saturnian E-ring (e.g., Hamilton and Burns 1994), whereby interplanetary EKB grains ejected from an earlier event have a non-negligible probability of impacting another EKBO. Given that impact ejecta yields can be

Table 2 Theoretical and observationally-constrained 0.1–10 μm dust production rates [$g\,s^{-1}$] from the Edgeworth-Kuiper Belt

Theoretical	
Stern (1996)	8.6×10^4–2.9×10^7
Yamamoto and Mukai (1998)	3.7×10^5–2.4×10^6
Observational	
Landgraf et al. (2002)	5×10^7
Han et al. (2011)	9×10^5
Vitense et al. (2012)	2×10^6
Poppe (2016)	6×10^6–1×10^7

significantly larger than unity even for the relatively low relative impact speeds in the EKB (Koschny and Grün 2001a), interplanetary dust grain bombardment may be an important process. Indeed, Poppe (2015) estimated that interplanetary dust bombardment produces between 3 and 200 times the amount of escaping ejecta from the Pluto-Charon system than does interstellar bombardment; however, it is currently unclear how this process compares to ISD bombardment when extrapolated over the entire EKB population.

Comparison between dynamical dust models (Landgraf et al. 2002; Han et al. 2011; Vitense et al. 2012; Poppe 2016) and in-situ dust flux measurements by several spacecraft, including Pioneer 10 and 11 (Humes 1980), Voyager 1 and 2 (Gurnett et al. 1997), Galileo (Sremčević et al. 2005), and New Horizons (Poppe et al. 2010; Szalay et al. 2013), have placed constraints on the total dust production rate from the EKB between 0.1 and 1.0 μm, listed in Table 2. In general, these observations are remarkably consistent with theoretical predictions.

7 Electrostatically Lofted Dust

In addition to impact processes which eject dust from airless bodies, there has been evidence for electrostatic processes contributing to the evolution and transport of dust on airless bodies. Electrostatic dust mobilization on the lunar surface has remained a controversial topic since the Apollo era. In situ and/or low-altitude observations (Rennilson and Criswell 1974; Severny et al. 1975; Berg 1978; Grün and Horányi 2013) as well as high-altitude remote sensing observations (McCoy and Criswell 1974; McCoy 1976; Glenar et al. 2011) have potentially suggested efficient lofting of charged dust particles near the lunar terminators.

One example of evidence for such a process occurring at low altitudes is from images taken just after sunset by the Surveyors 5, 6, and 7 cameras. In many of these images, a horizon glow was observed due west (Rennilson and Criswell 1974; Colwell et al. 2007a), an example of which is shown in Fig. 10. This glow has been interpreted as forward scattered light from a cloud of dust particles levitating less than 1 meter above the surface with particle radii on the order of 5 μm (Rennilson and Criswell 1974). However, as of yet, no mechanism capable of generating sufficiently large electric fields or dust grain charges to levitate such heavy particles has been identified (Hartzell and Scheeres 2011). The Lunar Ejecta and Meteorites experiment (LEAM) registered a multitude of unexpected hits during lunar sunrise and sunset (Berg et al. 1976), however, recent analysis suggests these signals were not caused by slow moving and highly charged dust grains transported across the lunar surface (Grün and Horányi 2013).

Features on asteroid (433) Eros that morphologically resembled ponds (Fig. 10) may indicate that small-scale electrostatic mobilization is a significant process on asteroidal sur-

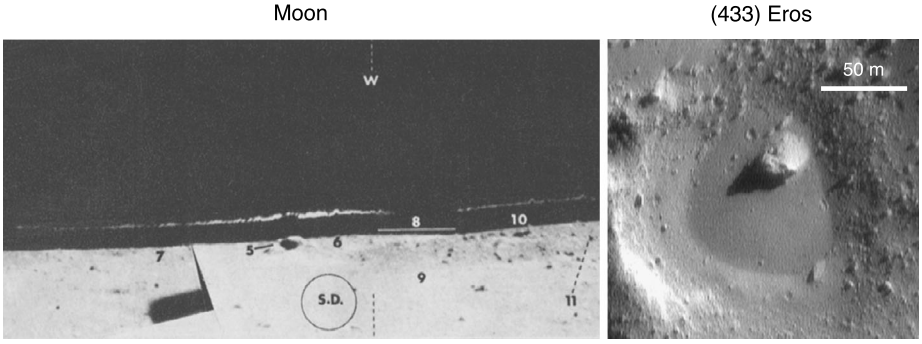

Fig. 10 Examples of possible evidence for electrostatic dust phenomena on airless bodies. *Left.* Surveyor 7 image showing horizon glow just after sunset. The sunlit foreground has been superimposed to show the surface features of the Moon relative to the putative levitated dust cloud. *Reproduced from Rennilson and Criswell (1974) with permission from Earth, Moon, and Planets. Right.* An example of dust ponds on (433) Eros, consisting of smooth, fine grained surface features that are suggested to be formed due to electrostatic mobilization and accumulation in crater depressions. *Reproduced from Richardson et al. (2005) with permission from Icarus*

faces (Veverka et al. 2001; Hughes et al. 2008; Thomas et al. 2015). We note that a competing theory suggests boulder erosion could lead to a similar phenomena (Dombard et al. 2010). Observations of Saturn's small moon Atlas have also suggested similar electrostatic processes occur (Hirata and Miyamoto 2012). For airless bodies with relatively low gravity, electrostatic transport may be part of the process that depletes surface dust (Lee 1996). Recent laboratory studies have shown that dust exposed to UV light and/or incident plasma experiences a high degree of small-scale mobilization and transport (Wang et al. 2009, 2010, 2011, 2016). Dust cohesion may also play an important role in dictating the dynamics of electrostatically lofted dust (Hartzell and Scheeres 2011; Hartzell et al. 2013).

Several decades of modeling efforts have addressed the theoretical possibility of electrostatic dust levitation and/or transport at airless bodies such as asteroids, the Moon, and the rings of Saturn. Early work, motivated by the Apollo observations by LEAM and Surveyor, focused on the possibility that intense electric fields may develop near the terminator regions of airless bodies as sunlit and shadowed portions of the surface lay in close proximity (e.g., De and Criswell 1977; Criswell and De 1977; Pelizzari and Criswell 1978). In theory, photoelectrons emitted from a sunlit patch of surface may be recollected on neighboring shadowed regions, and thus, trapped and unable to return through the highly resistive lunar soil. These simulations suggested that electric fields in the terminator region could reach up to 3×10^5 V/m, many orders-of-magnitude higher than estimated near noon, thereby facilitating the mobilization of lunar dust grains. These early simulations suffered from a number of limitations, most notably the lack of charge neutralization currents from the solar wind electrons. Thus, despite these early predictions, it is unlikely that such strong electric fields develop near the lunar terminator region (see e.g., Poppe et al. 2012; Zimmerman et al. 2014; Piquette and Horányi 2017, and discussion below).

Later analytic models of the electrostatic environment above asteroids, the Moon, and the main rings of Saturn suggested the possibility that dust grains may become electrostatically "trapped" in non-monotonic electrostatic potential layers above a surface (Nitter and Havnes 1992; Nitter et al. 1994, 1998) or preferentially deposited in craters due to differing surface electric fields (Colwell et al. 2005, 2009; Hughes et al. 2008). Farrell et al. (2007, 2008) explored the possibility that regions on the lunar surface just past the terminator may have

enhanced electric fields due to the presence of ambipolar separation of solar wind electrons and ions on the edge of the lunar wake; however, in contrast to the supercharging electric fields estimates of $\sim 10^5$, this work derived maximum electric fields near the terminator region of less than 10 V/m.

More recent studies used one- and three-dimensional electrostatic particle-in-cell models to further quantify the lunar plasma sheath both on a flat surface and near the presence of a typical, 10-m sized crater (Poppe and Horányi 2010; Poppe et al. 2012; Piquette and Horányi 2017). Poppe and Horányi (2010) found that non-monotonic potentials can theoretically exist and be energetically preferred for the lunar sheath (in theory allowing for "trapping" of levitated dust grains); however, the electric field strengths proved too weak to stably levitate and/or transport grains larger than ≈ 0.1 μm. For bodies with low gravity, modeling efforts found significant ponding can occur in the shadowed regions of craters, with approximately an order of magnitude more accumulation predicted for small bodies like (433) Eros than at the Moon for similar crater morphologies and plasma conditions (Piquette and Horányi 2017). Grain sizes this small are unable to explain the estimation of 5–10 μm sized levitated dust grains from Surveyor observations (Rennilson and Criswell 1974; Colwell et al. 2007a). Additionally, Hartzell and Scheeres (2013) determined stability regions for electrostatically levitated dust grains. Most recently, Wang et al. (2016) has proposed a "patched surface charge" model that describes how individual micron and submicron sized dust grains may attain charges far in excess of that predicted from a simple application of Gauss' Law (Schwan et al. 2017), thereby allowing significant electrostatic acceleration of micron-sized and larger grains onto ballistic trajectories above a charged surface. Three-dimensional electrostatic simulations performed by Zimmerman et al. (2016) have begun to elucidate this microphysical charging process and may provide the explanation for efficient electrostatic dust transport on airless bodies throughout the solar system.

Lunar and asteroidal observations as well as laboratory experiments have all suggested that small-scale electrostatic mobilization and transport occurs on airless bodies throughout the solar system. However, this phenomenon represents an active field of research and our understanding of this process is continually evolving. While high altitude observations also indicated the existence of lofted dust at tens of km above the surface, the case for such a population is weaker than for low altitudes. The first high altitude, remote sensing optical observations were made during the Apollo 15–17 missions, which took a series of calibrated images to analyze the zodiacal light and the solar corona (McCoy 1976). Some of these images indicated an excess brightness that has been interpreted as forward scattered light from small grains with characteristic radii $a \simeq 0.1$ μm lofted over the terminator regions of the Moon by electrostatic effects. The density of such a dust population was first calculated to be on the order of 10^4 m^{-3} near the surface using Apollo data (McCoy 1976; Glenar et al. 2011). Recent remote sensing surveys by Clementine (Glenar et al. 2014) and LRO/LAMP (Feldman et al. 2014) have significantly lowered the upper limit of the lofted dust density to ~ 1 m^{-3} near the surface. While LDEX could not individually detect dust impacts from 0.1 μm grains, it was able to search for such a population by integrating the cumulative current of impact plasma (Horányi et al. 2014). From data taken throughout LADEE's $\sim 2{,}000$ sunrise terminator transits, LDEX put an in-situ upper limit on the dust density distribution of 40–100 m^{-3} (Szalay and Horányi 2015b).

8 Conclusions and Outlook

In this review paper, we have reviewed the current state of knowledge of dust processes occurring in the vicinity of airless bodies. There have been many advancements made in

our understanding of these processes in the last two decades, which subsequently opened up new open questions for future studies and measurements. We conclude here with a brief summary of the paper and discuss open issues looking forward.

Our understanding of asteroidal surface properties has been dramatically increased by Itokawa asteroidal samples from the Hayabusa mission. These samples have been studied using advanced ground-based laboratory techniques, the results of which suggest asteroidal surfaces may be continually refreshed over time. Advanced ground-based techniques have been developed, such as phase-resolved photometry and polarimetry, to characterize regolith properties remotely in lieu of having asteroidal samples to study in the lab. There are many upcoming missions, such as OSIRIS-REx and Hayabusa-2, that plan to return additional asteroidal samples to Earth, which will further refine our understanding of these bodies and the surface weathering processes occurring on objects with different compositions and morphologies.

Ejecta clouds around both the Galilean satellites and the Moon have been explored and characterized by in-situ dust detectors. The two datasets have illuminated the nature of dust ejecta clouds and opened up new lines of study related to these clouds. The difference between the inferred ejecta velocity distributions at the Moon and the Galilean satellites remains an open issue that may be resolved by the Surface Dust Analyzer (SUDA) aboard the Europa Clipper mission, set to launch in the early 2020's. This mission will probe Europa's ejecta cloud down to altitudes of 25 km, allowing for direct comparison between the Moon's and Europa's impact ejecta clouds. Additionally, LDEX for the very first time directly transited through dense ejecta plumes comprised of hundreds of impacts. Analysis of these impact plume observations is ongoing and could shed light into the substructure of impact ejecta plumes in a manner unique to dust detector data.

Airless bodies can also be a significant source of interplanetary dust. Due to the large yields for high velocity meteoroid impacts, airless bodies exposed to these impactors can effectively shed their regolith into the IDP population. Quantifying the primary mechanisms and total production rates of IDP production from airless bodies is an important on-going research topic. In the inner solar system, such research is progressing somewhat faster, while in the outer solar system, greater uncertainty persists. Additionally, recent observational campaigns have been unraveling the mystery of active asteroids, which also produce interplanetary dust in characteristically different ways than comets. The relative importance of collisions and rotational disruption for activation of asteroids is a topic of ongoing research.

Electrostatic dust related processes have been a controversial topic since the Apollo era. Such phenomena can be divided into low-altitude and high-altitude populations. As our analysis tools and datasets have evolved, evidence for a high altitude population has continued to look less promising. However, recent laboratory measurements indicate that small-scale electrostatic dust mobilization is likely to occur at all airless bodies in the solar system. Future surface-based instrumentation suites, that would combine dust and plasma measurements, would greatly increase our understanding of these small-scale processes.

Acknowledgements The authors gratefully acknowledge the support of ISSI to produce this review paper. JRS was also supported by NASA's Lunar Data Analysis Program, Grant 80NSSC17K0702. ARP acknowledges NASA Planetary Atmospheres grant #NNX13AG55G and the NASA SSERVI Institute, grant #NNX14AG16A. We thank two anonymous reviewers for their constructive comments evaluating this paper.

References

J. Agarwal, M. Mommert, The nucleus of active asteroid 358P/Pan-STARRS (P/2012 T1). Astron. Astrophys. **549**, 357–359 (2017). https://doi.org/10.1038/nature23892

J. Agarwal, M. Müller, W.T. Reach, M.V. Sykes, H. Boehnhardt, E. Grün, The dust trail of Comet 67P/Churyumov-Gerasimenko between 2004 and 2006. Icarus **207**, 992–1012 (2010). https://doi.org/10.1016/j.icarus.2010.01.003

J. Agarwal, D. Jewitt, H. Weaver, Dynamics of large fragments in the tail of active asteroid P/2010 A2. Astrophys. J. **769**(1), 46 (2013)

J. Agarwal, D. Jewitt, H. Weaver, M. Mutchler, S. Larson, Hubble and Keck Telescope observations of active asteroid 288P/300163 (2006 VW139). Astron. J. **151**(1), 12 (2015)

J. Agarwal, D.C. Jewitt, M. Mutchler, H. Weaver, S. Larson, A binary main-belt comet. Nature **549**(7672), 357–359 (2017)

J.R. Arnold, A Monte Carlo model for the gardening of the lunar regolith. Moon **13**, 159–172 (1975)

N. Asada, Fine fragments in high-velocity impact experiments. J. Geophys. Res. **90**, 12445 (1985). https://doi.org/10.1029/JB090iB14p12445

E. Asphaug, S.J. Ostro, R. Hudson, D.J. Scheeres, W. Benz, Disruption of kilometre-sized asteroids by energetic collisions. Nature **393**(6684), 437 (1998)

F. Bagenal, M. Horányi, D.J. McComas, R.L. McNutt, H.A. Elliot, M.E. Hill, L.E. Brown, P.A. Delamere, P. Kollman, S.M. Krimigis, M. Kusterer, C.M. Lisse, D.G. Mitchell, M. Piquette, A.R. Poppe, D.F. Strobel, J.R. Szalay, P. Valek, J. Vandegriff, S. Weidner, E.J. Zirnstein, S.A. Stern, K. Ennico, C.B. Olkin, H.A. Weaver, L.A. Young, N.H.S. Team, Pluto's interaction with its space environment: Solar wind, energetic particles, and dust. Science **351**(6279), aad9045 (2016)

S. Barabash, R. Lundin, On a possible dust-plasma interaction at Mars. IEEE Trans. Plasma Sci. **22**(2), 173–178 (1994)

I. Belskaya, S. Bagnulo, Transneptunian objects and centaurs, in *Polarimetry of Stars and Planetary Systems*, ed. by L. Kolokolova, J. Hough, A.-C. Levasseur-Regourd (2015), p. 405

I.N. Belskaya, S. Bagnulo, M.A. Barucci, K. Muinonen, G.P. Tozzi, S. Fornasier, L. Kolokolova, Polarimetry of centaurs (2060) Chiron, (5145) Pholus and (10199) Chariklo. Icarus **210**(1), 472–479 (2010). https://doi.org/10.1016/j.icarus.2010.06.005. http://www.sciencedirect.com/science/article/pii/S0019103510002277

I. Belskaya, A. Cellino, R. Gil-Hutton, K. Muinonen, Y. Shkuratov, Asteroid polarimetry, in *Asteroids IV*, ed. by P. Michel, F.E. DeMeo, W.F. Bottke (2015), pp. 151–163

S.D. Benecchi, K.S. Noll, W.M. Grundy, H.F. Levison, (47171) 1999 TC_{36}, a transneptunian triple. Icarus **207**, 978–991 (2010)

A.A. Berezhnoy, E.A. Kozlova, M.P. Sinitsyn, A.A. Shangaraev, V.V. Shevchenko, Origin and stability of lunar polar volatiles. Adv. Space Res. **50**, 1638–1646 (2012)

O.E. Berg, Lunar terminator configuration. Earth Planet. Sci. Lett. **39**(3), 377–381 (1978)

O.E. Berg, H. Wolf, J. Rhee, Lunar soil movement registered by the Apollo 17 cosmic dust experiment, in *Interplanetary Dust and Zodiacal Light*, ed. by H. Elsaesser, H. Fechtig Lecture Notes in Physics, vol. 48 (Springer, Berlin, 1976), pp. 233–237

R. Berisch, W. Eckstein (eds.), *Sputtering by Particle Bombardment: Experiments and Computer Calculations from Threshold to MeV Energies*. Topics in Applied Physics, vol. 110 (Springer, Berlin, 2007)

J.P. Biersack, W. Eckstein, Sputtering studies with the Monte Carlo program TRIM.SP. Appl. Phys. A **34**, 73–94 (1984)

T. Birnstiel, H. Klahr, B. Ercolano, A simple model for the evolution of the dust population in protoplanetary disks. Astron. Astrophys. **539**, 148 (2012)

D. Bodewits, M. Kelley, J.-Y. Li, W. Landsman, S. Besse, M. A'Hearn, Collisional excavation of asteroid (596) Scheila. Astrophys. J. Lett. **733**(1), 3 (2011)

D. Bodewits, J.-B. Vincent, M.S. Kelley, Scheila's scar: direct evidence of impact surface alteration on a primitive asteroid. Icarus **229**, 190–195 (2014)

P. Borin, G. Cremonese, F. Marzari, M. Bruno, S. Marchi, Statistical analysis of micrometeoroids flux on Mercury. Astron. Astrophys. **503**, 259–264 (2009)

P. Borin, G. Cremonese, F. Marzari, Statistical analysis of the flux of micrometeoroids at Mercury from both cometary and asteroidal components. Astron. Astrophys. **585**, A106 (2016)

W.F. Bottke, M.C. Nolan, R. Greenberg, R.A. Kolvoord, Velocity distributions among colliding asteroids. Icarus **107**(2), 255–268 (1994)

W.F. Bottke, D. Vokrouhlicky, D.P. Rubincam, M. Broz, The effect of Yarkovsky thermal forces on the dynamical evolution of asteroids and meteoroids, in *Asteroids III* (2002), p. 395

W.F. Bottke, D.D. Durda, D. Nesvorný, R. Jedicke, A. Morbidelli, D. Vokrouhlický, H.F. Levison, Linking the collisional history of the main asteroid belt to its dynamical excitation and depletion. Icarus **179**(1), 63–94 (2005)

D. Britt, C. Pieters, Darkening in black and gas-rich ordinary chondrites: The spectral effects of opaque morphology and distribution. Geochim. Cosmochim. Acta **58**(18), 3905–3919 (1994)

M.E. Brown, W.M. Calvin, Evidence for crystalline water and ammonia ices on Pluto's satellite Charon. Science **287**, 107–109 (2000)
R. Brunetto, M.J. Loeffler, D. Nesvorný, S. Sasaki, G. Strazulla, Asteroid surface alteration by space weathering processes, in *Asteroids IV* (2015), pp. 597–616
E. Buhl, F. Sommer, M.H. Poelchau, G. Dresen, T. Kenkmann, Ejecta from experimental impact craters: particle size distribution and fragmentation energy. Icarus **237**, 131–142 (2014). https://doi.org/10.1016/j.icarus.2014.04.039
J.A. Burns, M. Showalter, D.P. Hamilton, P.D. Nicholson, I. de Pater, M.E. Ockert-Bell, P.C. Thomas, The formation of Jupiter's faint rings. Science **284**, 1146–1150 (1999)
M.D. Campbell-Brown, High resolution radiant distribution and orbits of sporadic radar meteoroids. Icarus **196**, 144–163 (2008). https://doi.org/10.1016/j.icarus.2008.02.022
P. Carrez, K. Demyk, P. Cordier, L. Gengembre, J. Grimblot, L. D'Hendecourt, A.P. Jones, H. Leroux, Low-energy helium ion irradiation-induced amorphization and chemical changes in olivine: insights for silicate dust evolution in the interstellar medium. Meteorit. Planet. Sci. **37**(11), 1599–1614 (2002)
R. Christoffersen, D.S. McKay, L.P. Keller, Microstructure, chemistry, and origin of grain rims on ilmenite from the lunar soil finest fraction. Meteorit. Planet. Sci. **31**(6), 835–848 (1996)
M.J. Cintala, Impact-induced thermal effects in the Lunar and Mercurian regoliths. J. Geophys. Res. **97**(E1), 947–973 (1992)
F. Cipriani, O. Witasse, F. Leblanc, R. Modolo, R.E. Johnson, A model of interaction of Phobos' surface with the Martian environment. Icarus **212**, 643–648 (2011)
R.N. Clark, J.M. Curchin, R. Jaumann, D.P. Cruikshank, R.H. Brown, T.M. Hoefen, K. Stephan, J.M. Moore, B.J. Buratti, K.H. Baines, P.D. Nicholson, R.M. Nelson, Compositional mapping of Saturn's satellite Dione with Cassini VIMS and implications of dark material in the Saturn system. Icarus **193**, 372–386 (2008)
R.N. Clark, D.P. Cruikshank, R. Jaumann, R.H. Brown, K. Stephan, C.M. Dalle Ore, K.E. Livo, N. Pearson, J.M. Curchin, T.M. Hoefen, B.J. Buratti, G. Filacchione, K.H. Baines, P.D. Nicholson, The surface composition of Iapetus: mapping results from Cassini VIMS. Icarus **218**, 831–860 (2012)
A. Colaprete et al., Detection of water in the LCROSS ejecta plume. Science **330**(6003), 463–468 (2010)
A. Colaprete, M. Sarantos, D.H. Wooden, T.J. Stubbs, A.M. Cook, M. Shirley, How surface composition and meteoroid impacts mediate sodium and potassium in the lunar exosphere. Science **351**(6270), 249–252 (2016)
A. Collette, K. Drake, A. Mocker, Z. Sternovsky, T. Munsat, M. Horányi, Time-resolved temperature measurements in hypervelocity dust impacts. Planet. Space Sci. **89**, 58–62 (2013)
A. Collette, Z. Sternovsky, M. Horányi, Production of neutral gas by micrometeoroid impacts. Icarus **227**, 89–93 (2014)
G. Colombo, D.A. Lautman, I.I. Shapiro, The Earth's Dust Belt: Fact or fiction?: 2. Gravitational focusing and Jacobi capture. J. Geophys. Res. **71**, 5705–5717 (1966). https://doi.org/10.1029/JZ071i023p05705
J.E. Colwell, A.A.S. Gulbis, M. Horányi, S. Robertson, Dust transport in photoelectron layers and the formation of dust ponds on Eros. Icarus **175**, 159–169 (2005)
J.E. Colwell, M. Horányi, S. Robertson, X. Wang, A. Haugsjaa, P. Wheeler, Behavior of charged dust in plasma and photoelectron sheaths, in *Dust in Planetary Systems*. ESA SP, vol. 643 (2007a), pp. 171–175
J.E. Colwell, S. Robertson, M. Horányi, X. Wang, A. Poppe, P. Wheeler, Lunar dust levitation. J. Aerosp. Eng. **1**, 2–9 (2009)
J.C. Cook, S.J. Desch, T.L. Roush, C.A. Trujillo, T.R. Geballe, Near-infrared spectroscopy of Charon: possible evidence for cryovolcanism on Kuiper Belt Objects. Astrophys. J. **663**, 1406–1419 (2007)
D. Crider, R.M. Killen, Burial rate of Mercury's polar volatile deposits. Geophys. Res. Lett. **32**, L12201 (2005)
D.H. Crider, R.R. Vondrak, Space weathering effects on lunar cold trap deposits. J. Geophys. Res. **108**(E7), 5079 (2003)
D.R. Criswell, B.R. De, Intense localized photoelectric charging in the Lunar sunset terminator region: 2. Supercharging at the progression of sunset. J. Geophys. Res. **82**(7), 1005–1007 (1977)
D.P. Cruikshank, J.F. Bell, M.J. Gaffey, R.H. Brown, R. Howell, C. Beerman, M. Rognstad, The dark side of Iapetus. Icarus **53**, 90–104 (1983)
C.M. Dalle Ore, D.P. Cruikshank, R.N. Clark, Infrared spectroscopic characterization of the low-albedo materials on Iapetus. Icarus **221**, 735–743 (2012)
C.M. Dalle Ore, D.P. Cruikshank, R.M.E. Mastrapa, E. Lewis, O.L. White, Impact craters: an icy study on Rhea. Icarus **261**, 80–90 (2015)
D.R. Davis, P. Farinella, Collisional evolution of Edgeworth-Kuiper belt objects. Icarus **125**, 50–60 (1997)
G. de Elía, A. Brunini, Collisional and dynamical evolution of the L_4 Trojan asteroids. Astron. Astrophys. **475**(1), 375–389 (2007)

I. de Pater, S.G. Gibbard, H.B. Hammel, Evolution of the dusty rings of Uranus. Icarus **180**, 186–200 (2006a)
I. de Pater, H.B. Hammel, S.G. Gibbard, M.R. Showalter, New dust belts of Uranus: one ring, two ring, red ring, blue ring. Science **312**, 92–94 (2006b)
B.R. De, D.R. Criswell, Intense localized photoelectric charging in the lunar sunset terminator region: 1. Development of potentials and fields. J. Geophys. Res. **82**(7), 999–1004 (1977)
M. Delbo, G. Libourel, J. Wilkerson, N. Murdoch, P. Michel, K. Ramesh, C. Ganino, C. Verati, S. Marchi, Thermal fatigue as the origin of regolith on small asteroids. Nature **508**(7495), 233–236 (2014)
M. Delbo, M. Mueller, J.P. Emery, B. Rozitis, M.T. Capria, Asteroid thermophysical modeling, in *Asteroids IV* (2015), p. 107
F. DeMeo, C. Alexander, K. Walsh, C. Chapman, R. Binzel, The compositional structure of the asteroid belt, in *Asteroids IV* (2015b), pp. 13–42
L. Denneau, R. Jedicke, A. Fitzsimmons, H. Hsieh, J. Kleyna, M. Granvik, M. Micheli, T. Spahr, P. Vereš, R. Wainscoat, et al., Observational constraints on the catastrophic disruption rate of small main belt asteroids. Icarus **245**, 1–15 (2015)
S.J. Desch, M. Neveu, Differentiation and cryovolcanism on Charon: a view before and after New Horizons. Icarus **287**, 175–186 (2017)
S.J. Desch, J.C. Cook, T.C. Doggett, S.B. Porter, Thermal evolution of Kuiper belt objects, with implications for cryovolcanism. Icarus **202**, 694–714 (2009)
V. Dikarev, E. Grün, J. Baggaley, D. Galligan, M. Landgraf, R. Jehn, The new ESA meteoroid model. Adv. Space Res. **35**(7), 1282–1289 (2005)
N. Divine, Five populations of interplanetary meteoroids. J. Geophys. Res. **98**, 17029–17048 (1993). https://doi.org/10.1029/93JE01203
A.V. Dmitriev, A.V. Suvorova, I.S. Veselovsky, Statistical Characteristics of the Heliospheric Plasma and Magnetic Field at Earth's Orbit during Four Solar Cycles 20-23, in *Handbook on Solar Wind: Effects, Dynamics, and Interactions*, ed. by H.E. Johannson (NOVA Science Publishers, New York, 2011), pp. 81–144. Chap. 2
A.J. Dombard, O.S. Barnouin, L.M. Prockter, P.C. Thomas, Boulders and ponds on the Asteroid 433 Eros. Icarus **210**(2), 713–721 (2010)
M. Drahus, W. Waniak, S. Tendulkar, J. Agarwal, D. Jewitt, S.S. Sheppard, Fast rotation and trailing fragments of the active asteroid P/2012 F5 (Gibbs). Astrophys. J. Lett. **802**(1), 8 (2015)
E. Dubinin, R. Lundin, N.F. Pissarenko, S.V. Barabash, A.V. Zakharov, H. Koskinen, K. Schwingenschuh, Y.G. Yeroshenko, Indirect evidences for a gas/dust torus along the Phobos orbit. Geophys. Res. Lett. **17**(6), 861–864 (1990)
E.M. Dubinin, N.F. Pissarenko, S.V. Barabash, A.V. Zakharov, R. Lundin, R. Pellinen, K. Schwingenschuh, Plasma and magnetic field effects associated with Phobos and Deimos tori. Planet. Space Sci. **39**(1/2), 113–121 (1991)
D.D. Durda, S.A. Stern, Collision rates in the present-day Kuiper belt and Centaur regions: applications to surface activation and modification on comets, Kuiper belt objects, Centaurs, and Pluto-Charon. Icarus **145**, 220–229 (2000)
R.C. Elphic, G.T. Delory, B.P. Hine, P. Mahaffy, M. Horanyi, A. Colaprete, M. Benna, S. Noble, The Lunar Atmosphere and Dust Environment Explorer Mission. Space Sci. Rev. **185**, 3–25 (2014)
W.M. Farrell, T.J. Stubbs, R.R. Vondrak, G.T. Delory, J.S. Halekas, Complex electric fields near the lunar terminator: the near-surface wake and accelerated dust. Geophys. Res. Lett. **34**, L14201 (2007)
W.M. Farrell, T.J. Stubbs, J.S. Halekas, G.T. Delory, M.R. Collier, R.R. Vondrak, R.P. Lin, Loss of solar wind plasma neutrality and affect on surface potentials near the lunar terminator and shadowed polar regions. Geophys. Res. Lett. **35**, L05105 (2008)
P.D. Feldman, D.A. Glenar, T.J. Stubbs, K.D. Retherford, G. Randall Gladstone, P.F. Miles, T.K. Greathouse, D.E. Kaufmann, J.W. Parker, S. Alan Stern, Upper limits for a lunar dust exosphere from far-ultraviolet spectroscopy by LRO/LAMP. Icarus **233**, 106–113 (2014)
M. Finson, R. Probstein, A theory of dust comets. I. Model and equations. Astrophys. J. **154**, 327–352 (1968)
A. Fujiwara, J. Kawaguchi, D.K. Yeomans, M. Abe, T. Mukai, T. Okada, J. Saito, H. Yano, M. Yoshikawa, D.J. Scheeres, O. Barnouin-Jha, A.F. Cheng, H. Demura, R.W. Gaskell, N. Hirata, H. Ikeda, T. Kominato, H. Miyamoto, A.M. Nakamura, R. Nakamura, S. Sasaki, K. Uesugi, The rubble-pile asteroid Itokawa as observed by Hayabusa. Science **312**, 1330–1334 (2006). https://doi.org/10.1126/science.1125841
M. Fulle, L. Colangeli, J. Agarwal, A. Aronica, V. Della Corte, F. Esposito, E. Grün, M. Ishiguro, R. Ligustri, J.J. Lopez Moreno, E. Mazzotta Epifani, G. Milani, F. Moreno, P. Palumbo, J. Rodríguez Gómez, A. Rotundi, Comet 67P/Churyumov-Gerasimenko: the GIADA dust environment model of the Rosetta mission target. Astron. Astrophys. **522**, 63 (2010). https://doi.org/10.1051/0004-6361/201014928
E. Füri, B. Marty, S.S. Assonov, Constraints on the flux of meteoritic and cometary water on the Moon from volatile element (N-Ar) analysis of single lunar soil grains, Luna 24 core. Icarus **218**, 220–229 (2012)

D.E. Gault, F. Hörz, D.E. Brownlee, J.B. Hartung, Mixing of the lunar regolith, in *Proc. 5th Lunar Conf.*, vol. 5 (1974)
B. Gladman, P. Michel, C. Froeschlé, The near-Earth object population. Icarus **146**(1), 176–189 (2000)
D.A. Glenar, T.J. Stubbs, J.E. McCoy, R.R. Vondrak, A reanalysis of the Apollo light scattering observations, and implications for lunar exospheric dust. Planet. Space Sci. **59**, 1695–1707 (2011)
D.A. Glenar, T.J. Stubbs, M. Hahn, Y. Wang, Search for a high altitude lunar dust exosphere using Clementine navigational star tracker measurements. J. Geophys. Res. **119**, 2548–2567 (2014)
C.A. Goodrich, E.R. Scott, A.M. Fioretti, Ureilitic breccias: clues to the petrologic structure and impact disruption of the ureilite parent asteroid. Chem. Erde **64**(4), 283–327 (2004)
E. Grün, M. Horányi, A new look at Apollo 17 LEAM data: nighttime dust activity in 1976. Planet. Space Sci. **89**, 2–14 (2013). https://doi.org/10.1016/j.pss.2013.10.005
E. Grün, H. Fechtig, M.S. Hanner, J. Kissel, B.-A. Lindblad, D. Linkert, D. Maas, G.E. Morfill, H.A. Zook, The Galileo dust detector. Space Sci. Rev. **60**, 317–340 (1992). https://doi.org/10.1007/BF00216860
E. Grün, B. Gustafson, I. Mann, M. Baguhl, G.E. Morfill, P. Staubach, A. Taylor, H.A. Zook, Interstellar dust in the heliosphere. Astron. Astrophys. **286**, 915–924 (1994)
W.M. Grundy, M.W. Buie, J.A. Stansberry, J.R. Spencer, B. Schmitt, Near-infrared spectra of icy outer Solar System surfaces: remote determination of H_2O ice temperatures. Icarus **142**, 536–549 (1999)
B. Gundlach, J. Blum, A new method to determine the grain size of planetary regolith. Icarus **223**(1), 479–492 (2013)
D.A. Gurnett, J.A. Ansher, W.S. Kurth, L.J. Granroth, Micron-sized dust particles detected in the outer solar system by the Voyager 1 and 2 plasma wave instruments. Geophys. Res. Lett. **24**(24), 3125–3128 (1997)
J.M. Hahn, H.A. Zook, B. Cooper, B. Sunkara, Clementine observations of the zodiacal light and the dust content of the inner solar system. Icarus **158**, 360–378 (2002)
O. Hainaut, J. Kleyna, G. Sarid, B. Hermalyn, A. Zenn, K. Meech, P. Schultz, H. Hsieh, G. Trancho, J. Pittichová, et al., P/2010 A2 LINEAR-I. An impact in the asteroid main belt. Astron. Astrophys. **537**, 69 (2012)
O. Hainaut, H. Boehnhardt, C. Snodgrass, K. Meech, J. Deller, M. Gillon, E. Jehin, E. Kuehrt, S. Lowry, J. Manfroid, et al., Continued activity in P/2013 P5 PANSTARRS—unexpected comet, rotational break-up, or rubbing binary asteroid? Astron. Astrophys. **563**, 75 (2014)
D.P. Hamilton, J.A. Burns, Origin of Saturn's E ring: self-sustained, naturally. Science **264**, 550–553 (1994)
D.P. Hamilton, H. Krüger, The sculpting of Jupiter's gossamer rings by its shadow. Nature **453**, 72–75 (2008)
D.P. Hamilton, M.F. Skrutskie, A.J. Verbiscer, F.J. Masci, Small particles dominate Saturn's Phoebe ring to surprisingly large distances. Nature **522**, 185–187 (2015)
D. Han, A.R. Poppe, M. Piquette, E. Grün, M. Horányi, Constraints on dust production in the Edgeworth-Kuiper Belt from Pioneer 10 and New Horizons measurement. Geophys. Res. Lett. **38**, L24102 (2011)
B. Hapke, Space weathering from Mercury to the asteroid belt. J. Geophys. Res. **106**(E), 10039–10074 (2001)
J.K. Harmon, M.A. Slade, M.S. Rice, Radar imagery of Mercury's putative polar ice: 1999–2005 Arecibo results. Icarus **211**, 37–50 (2011)
W.K. Hartmann, Impact experiments. I—Ejecta velocity distributions and related results from regolith targets. Icarus **63**, 69–98 (1985). https://doi.org/10.1016/0019-1035(85)90021-1
C.M. Hartzell, D.J. Scheeres, The role of cohesive forces in particle launching on the moon and asteroids. Planet. Space Sci. **59**(14), 1758–1768 (2011). Lunar Dust, Atmosphere and Plasma: The Next Steps
C.M. Hartzell, D.J. Scheeres, Dynamics of levitating dust particles near asteroids and the moon. J. Geophys. Res., Planets **118**(1), 116–125 (2013)
C.M. Hartzell, X. Wang, D.J. Scheeres, M. Horányi, Experimental demonstration of the role of cohesion in electrostatic dust lofting. Geophys. Res. Lett. **40**(6), 1038–1042 (2013)
P.O. Hayne, A. Hendrix, E. Sefton-Nash, M.A. Siegler, P.G. Lucey, K.D. Retherford, J.-P. Williams, B.T. Greenhagen, D.A. Paige, Evidence for exposed water ice in the Moon's south polar regions from Lunar Reconnaissance Orbiter ultraviolet albedo and temperature measurements. Icarus **255**, 58–69 (2015)
M.M. Hedman, C.D. Murray, N.J. Cooper, M.S. Tiscareno, K. Beurle, M.W. Evans, J.A. Burns, Three tenuous rings/arcs for three tiny moons. Icarus **199**, 378–386 (2009)
M. Hirabayashi, Failure modes and conditions of a cohesive, spherical body due to YORP spin-up. Mon. Not. R. Astron. Soc. **454**(2), 2249–2257 (2015)
M. Hirabayashi, D.J. Scheeres, Analysis of asteroid (216) Kleopatra using dynamical and structural constraints. Astrophys. J. **780**(2), 160 (2013)
N. Hirata, H. Miyamoto, Dust levitation as a major resurfacing process on the surface of a saturnian icy satellite, Atlas. Icarus **220**, 106–113 (2012)
M. Horányi, J.A. Burns, M. Tatrallyay, J.G. Luhmann, Toward understanding the fate of dust lost from the martian satellites. Geophys. Res. Lett. **17**(6), 853–856 (1990)
M. Horányi, M. Tatrallyay, A. Juhász, J.G. Luhmann, The dynamics of submicron-sized dust particles lost from Phobos. J. Geophys. Res. **96**(A7), 11283–11290 (1991)

M. Horányi, Z. Sternovsky, M. Lankton, C. Dumont, S. Gagnard, D. Gathright, E. Grün, D. Hansen, D. James, S. Kempf, B. Lamprecht, J. Szalay, R. Srama, G. Wright, The Lunar Dust Experiment (LDEX) onboard the Lunar Atmosphere and Dust Environment Explorer (LADEE) mission. Space Sci. Rev. **185**, 93–113 (2014)
M. Horányi, J.R. Szalay, S. Kempf, J. Schmidt, E. Grün, R. Srama, Z. Sternovsky, A permanent, asymmetric dust cloud around the Moon. Nature **522**(7556), 324 (2015)
J. Horner, N. Evans, M. Bailey, Simulations of the population of centaurs—I. the bulk statistics. Mon. Not. R. Astron. Soc. **354**(3), 798–810 (2004)
K.R. Housen, K.A. Holsapple, Ejecta from impact craters. Icarus **211**(1), 856–875 (2011)
H.H. Hsieh, D. Jewitt, A population of comets in the main asteroid belt. Science **312**(5773), 561–563 (2006)
H.H. Hsieh, D.C. Jewitt, Y.R. Fernández, The strange case of 133P/Elst-Pizarro: a comet among the asteroids. Astron. J. **127**(5), 2997 (2004)
H.H. Hsieh, D. Jewitt, M. Ishiguro, Physical properties of main-belt comet P/2005 U1 (Read). Astron. J. **137**(1), 157 (2008)
H.H. Hsieh, D. Jewitt, P. Lacerda, S.C. Lowry, C. Snodgrass, The return of activity in main-belt Comet 133P/Elst-Pizarro. Mon. Not. R. Astron. Soc. **403**, 363–377 (2010). https://doi.org/10.1111/j.1365-2966.2009.16120.x
H.H. Hsieh, M. Ishiguro, P. Lacerda, D. Jewitt, Physical properties of main-belt comet 176P/LINEAR. Astron. J. **142**(1), 29 (2011)
H.H. Hsieh, O. Hainaut, B. Novaković, B. Bolin, L. Denneau, A. Fitzsimmons, N. Haghighipour, J. Kleyna, R. Kokotanekova, P. Lacerda, et al., Sublimation-driven activity in main-belt comet 313P/Gibbs. Astrophys. J. Lett. **800**(1), 16 (2015)
A.L.H. Hughes, J.E. Colwell, A.W. Dewolfe, Electrostatic dust transport on Eros: 3-D simulations of pond formation. Icarus **195**, 630–648 (2008)
M.-T. Hui, D. Jewitt, Non-gravitational acceleration of the active asteroids. Astron. J. **153**(2), 80 (2017)
M.-T. Hui, D. Jewitt, X. Du, Split active asteroid P/2016 J1 (Panstarrs). Astron. J. **153**(4), 141 (2017). http://stacks.iop.org/1538-3881/153/i=4/a=141
D.H. Humes, Results of Pioneer 10 and 11 meteoroid experiments: interplanetary and near-Saturn. J. Geophys. Res. **85**(A11), 5841–5852 (1980)
D.M. Hunten, G. Cremonese, A.L. Sprague, R.E. Hill, S. Verani, R.W.H. Kozlowski, The Leonid meteor shower and the lunar sodium atmosphere. Icarus **136**, 298–303 (1998)
D.M. Hurley, D.J. Lawrence, D.B.J. Bussey, R.R. Vondrak, R.C. Elphic, G.R. Gladstone, Two-dimensional distribution of volatiles in the lunar regolith from space weathering simulations. Geophys. Res. Lett. **39**, L09203 (2012)
W.-H. Ip, M. Banaszkiewicz, On the dust/gas tori of Phobos and Deimos. Geophys. Res. Lett. **17**(6), 857–860 (1990)
M. Ishiguro, H. Hanayama, S. Hasegawa, Y. Sarugaku, J.-i. Watanabe, H. Fujiwara, H. Terada, H.H. Hsieh, J.J. Vaubaillon, N. Kawai, et al., Interpretation of (596) Scheila's triple dust tails. Astrophys. J. Lett. **741**(1), 24 (2011a)
M. Ishiguro, H. Hanayama, S. Hasegawa, Y. Sarugaku, J.-I. Watanabe, H. Fujiwara, H. Terada, H.H. Hsieh, J.J. Vaubaillon, N. Kawai, et al., Observational evidence for an impact on the main-belt Asteroid (596) Scheila. Astrophys. J. Lett. **740**(1), 11 (2011b)
H. Ishimoto, Formation of Phobos/Deimos dust rings. Icarus **122**, 153–165 (1996)
J. Jackson, Glossary of geology. Technical report. American Geological Institute, Alexandria, VA (1997), 769 pp., ISBN 0-922152-34-9
D. Janches, J.D. Mathews, D.D. Meisel, V.S. Getman, Q.H. Zhou, Doppler studies of near-antapex UHF radar micrometeors. Icarus **143**(2), 347–353 (2000)
D. Janches, P. Pokorný, M. Sarantos, J.R. Szalay, M. Horányi, D. Nesvorný, Constraining the ratio of micrometeoroids from short and long period comets at 1 AU from LADEE observations of the lunar dust cloud. Geophys. Res. Lett. (2018). https://doi.org/10.1002/2017GL076065.
P. Jenniskens, Meteoroid streams and the zodiacal cloud, in *Asteroids IV* (University of Arizona Press, Tucson, 2015), p. 281
P. Jenniskens, D.F. Blake, Crystallization of amorphous water ice in the Solar System. Astrophys. J. **473**, 1104–1113 (1996)
D. Jewitt, The active asteroids. Astron. J. **143**(3), 66 (2012)
D. Jewitt, J. Li, Activity in Geminid Parent (3200) Phaethon. Astron. J. **140**(5), 1519 (2010)
D.C. Jewitt, J.X. Luu, Crystalline water ice on the Kuiper belt object (50000) Quaoar. Nature **432**, 731–733 (2004)
D. Jewitt, B. Yang, N. Haghighipour, Main-belt comet P/2008 R1 (Garradd). Astron. J. **137**(5), 4313 (2009)
D. Jewitt, H. Weaver, J. Agarwal, M. Mutchler, M. Drahus, A recent disruption of the main-belt asteroid P/2010 A2. Nature **467**(7317), 817–819 (2010)

D. Jewitt, H. Weaver, M. Mutchler, S. Larson, J. Agarwal, Hubble Space Telescope observations of main-belt comet (596) Scheila. Astrophys. J. Lett. **733**(1), 4 (2011)
D. Jewitt, J. Agarwal, H. Weaver, M. Mutchler, S. Larson, The extraordinary multi-tailed main-belt Comet P/2013 P5. Astrophys. J. Lett. **778**(1), L21 (2013)
D. Jewitt, M. Ishiguro, J. Agarwal, Large particles in active asteroid P/2010 A2. Astrophys. J. Lett. **764**(1), 5 (2013a)
D. Jewitt, J. Li, J. Agarwal, The dust tail of asteroid (3200) Phaethon. Astrophys. J. Lett. **771**(2), 36 (2013b)
D. Jewitt, J. Agarwal, J. Li, H. Weaver, M. Mutchler, S. Larson, Disintegrating asteroid P/2013 R3. Astrophys. J. Lett. **784**(1), 8 (2014a)
D. Jewitt, M. Ishiguro, H. Weaver, J. Agarwal, M. Mutchler, S. Larson, Hubble Space Telescope investigation of main-belt comet 133P/Elst-Pizarro. Astron. J. **147**(5), 117 (2014b)
D. Jewitt, J. Agarwal, H. Weaver, M. Mutchler, S. Larson, Episodic ejection from active asteroid 311P/PANSTARRS. Astrophys. J. **798**(2), 109 (2015a)
D. Jewitt, J. Agarwal, N. Peixinho, H. Weaver, M. Mutchler, M.-T. Hui, J. Li, S. Larson, New active asteroid 313P/Gibbs. Astron. J. **149**(2), 81 (2015b)
D. Jewitt, J. Li, J. Agarwal, H. Weaver, M. Mutchler, S. Larson, Nucleus and mass loss from active asteroid 313P/Gibbs. Astron. J. **150**(3), 76 (2015c)
D. Jewitt, H. Hsieh, J. Agarwal, et al., The active asteroids, in *Asteroids IV* (University of Arizona, Tucson, 2015d), pp. 221–241
J. Jones, P. Brown, Sporadic meteor radiant distributions—orbital survey results. Mon. Not. R. Astron. Soc. **265**, 524 (1993)
A. Juhász, M. Horányi, Dust torus around Mars. J. Geophys. Res. **100**(E2), 3277–3284 (1995)
A. Juhász, M. Tátrallyay, G. Gévai, M. Horányi, On the density of the dust halo around Mars. J. Geophys. Res. **98**(E1), 1205–1211 (1993)
S. Kameda, I. Yoshikawa, M. Kagitani, S. Okano, Interplanetary dust distribution and temporal variability of Mercury's atmospheric Na. Geophys. Res. Lett. **36**, L15201 (2009)
L.P. Keller, E.L. Berger, A transmission electron microscope study of Itokawa regolith grains. Earth Planets Space **66**(1), 71 (2014)
L.P. Keller, D.S. McKay, The nature and origin of rims on lunar soil grains. Geochim. Cosmochim. Acta **61**(11), 2331–2341 (1997)
S. Kempf, Interpretation of high rate dust measurements with the Cassini dust detector CDA. Planet. Space Sci. **56**, 378–385 (2008). https://doi.org/10.1016/j.pss.2007.11.022
K.V. Kholshevnikov, A.V. Krivov, L.L. Sokolov, V.B. Titov, The dust torus around Phobos orbit. Icarus **105**, 351–362 (1993)
R.M. Killen, J.M. Hahn, Impact vaporization as a possible source of Mercury's calcium exosphere. Icarus **250**, 230–237 (2015)
R.M. Killen, W.-H. Ip, The surface-bounded atmosphere of Mercury and the Moon. Rev. Geophys. **37**(3), 361–406 (1999)
Y. Kim, M. Ishiguro, M.G. Lee, New observational evidence of active asteroid P/2010 A2: slow rotation of the largest fragment. Astrophys. J. Lett. **842**, 23 (2017a). https://doi.org/10.3847/2041-8213/aa7944
Y. Kim, M. Ishiguro, T. Michikami, A.M. Nakamura, Anisotropic ejection from active asteroid P/2010 A2: an implication of impact shattering on an asteroid. Astron. J. **153**, 228 (2017b). https://doi.org/10.3847/1538-3881/aa69bb
H. Kosai, Short-period comets and Apollo-Amor-Aten type asteroids in view of Tisserand invariant, in *Dynamics and Evolution of Minor Bodies with Galactic and Geological Implications* (Springer, Berlin, 1992), pp. 237–240
D. Koschny, E. Grün, Impacts into ice-silicate mixtures: crater morphologies, volumes, depth-to-diameter ratios, and yield. Icarus **154**, 391–401 (2001a)
D. Koschny, E. Grün, Impacts into ice-silicate mixtures: ejecta mass and size distributions. Icarus **154**, 402–411 (2001b). https://doi.org/10.1006/icar.2001.6708
L. Kresak, On the similarity of orbits of associated comets, asteroids and meteoroids. Bull. Astron. Inst. Czechoslov. **33**, 104–110 (1982)
A.V. Krivov, On the dust belts of Mars. Astron. Astrophys. **291**, 657–663 (1994)
A.V. Krivov, D.P. Hamilton, Martian dust belts: waiting for discovery. Icarus **128**, 335–353 (1997)
A. Krivov, A. Jurewicz, The ethereal dust envelopes of the Martian moons. Planet. Space Sci. **47**, 45–56 (1998). https://doi.org/10.1016/S0032-0633(98)00101-9
A.V. Krivov, H. Krüger, E. Grün, K.-U. Thiessenhusen, D.P. Hamilton, A tenuous dust ring of Jupiter formed by escaping ejecta from the Galilean satellites. J. Geophys. Res., Planets **107**, 5002 (2002). https://doi.org/10.1029/2000JE001434
A.V. Krivov, M. Sremčević, F. Spahn, V.V. Dikarev, K.V. Kholshevnikov, Impact-generated dust clouds around planetary satellites: spherically symmetric case. Planet. Space Sci. **51**, 251–269 (2003)

A.V. Krivov, A.G. Feofilov, V.V. Dikarev, Search for the putative dust belts of Mars: The late 2007 opportunity. Planet. Space Sci. **54**, 871–878 (2006)
H. Krüger, E. Grün, Interstellar dust inside and outside the heliosphere. Space Sci. Rev. **143**, 347–356 (2009)
H. Krüger, A.V. Krivov, D.P. Hamilton, E. Grün, Detection of an impact-generated dust cloud around Ganymede. Nature **399**, 558–560 (1999). https://doi.org/10.1038/21136
H. Krüger, A.V. Krivov, E. Grün, A dust cloud of Ganymede maintained by hypervelocity impacts of interplanetary micrometeoroids. Planet. Space Sci. **48**, 1457–1471 (2000). https://doi.org/10.1016/S0032-0633(00)00092-1
H. Krüger, A.V. Krivov, M. Sremčević, E. Grün, Impact-generated dust clouds surrounding the Galilean moons. Icarus **164**(1), 170–187 (2003)
H. Krüger et al., Interstellar dust in the solar system. Space Sci. Rev. **130**(1–4), 401–408 (2007)
H. Krüger, P. Strub, E. Grün, V.J. Sterken, Sixteen years of Ulysses interstellar dust measurements in the Solar System. I. Mass distribution and gas-to-dust mass ratio. Astrophys. J. **812**(2), 1–16 (2015)
M. Landgraf, J.-C. Liou, H.A. Zook, E. Grün, Origins of solar system dust beyond Jupiter. Astron. J. **123**, 2857–2861 (2002)
D.S. Lauretta, A.E. Bartels, M.A. Barucci, E.B. Bierhaus, R.P. Binzel, W.F. Bottke, H. Campins, S.R. Chesley, B.C. Clark, B.E. Clark, E.A. Cloutis, H.C. Connolly, M.K. Crombie, M. Delbó, J.P. Dworkin, J.P. Emery, D.P. Glavin, V.E. Hamilton, C.W. Hergenrother, C.L. Johnson, L.P. Keller, P. Michel, M.C. Nolan, S.A. Sandford, D.J. Scheeres, A.A. Simon, B.M. Sutter, D. Vokrouhlický, K.J. Walsh, The OSIRIS-REx target asteroid (101955) Bennu: constraints on its physical, geological, and dynamical nature from astronomical observations. Meteorit. Planet. Sci. **50**(4), 834–849 (2015). https://doi.org/10.1111/maps.12353
P. Lee, Dust levitation on asteroids. Icarus **124**, 181–194 (1996). https://doi.org/10.1006/icar.1996.0197
E. Lellouch, P. Santos-Sanz, P. Lacerda, M. Mommert, R. Duffard, J. Ortiz, T. Müller, S. Fornasier, J. Stansberry, C. Kiss, et al., "TNOs are Cool": a survey of the trans-Neptunian region-IX. Thermal properties of Kuiper belt objects and Centaurs from combined Herschel and Spitzer observations. Astron. Astrophys. **557**, 60 (2013)
G. Leto, G.A. Baratta, Ly-α photon induced amorphization of Ic water ice at 16 Kelvin. Astron. Astrophys. **397**, 7–13 (2003)
H.F. Levison, E.M. Shoemaker, C.S. Shoemaker, Dynamical evolution of Jupiter's Trojan asteroids. Nature **385**(6611), 42 (1997)
H.F. Levison, A. Morbidelli, C. VanLaerhoven, R. Gomes, K. Tsiganis, Origin of the structure of the Kuiper belt during a dynamical instability in the orbits of Uranus and Neptune. Icarus **196**(1), 258–273 (2008)
H.F. Levison, K.A. Kretke, M.J. Duncan, Growing the gas-giant planets by the gradual accumulation of pebbles. Nature **524**(7565), 322–324 (2015)
J. Li, D. Jewitt, Recurrent perihelion activity in (3200) Phaethon. Astron. J. **145**(6), 154 (2013)
J. Licandro, F. Moreno, J. de León, G. Tozzi, L. Lara, A. Cabrera-Lavers, Exploring the nature of new main-belt comets with the 10.4 m GTC telescope: (300163) 2006 VW139. Astron. Astrophys. **550**, A17 (2013)
J.-C. Liou, H.A. Zook, Signatures of the giant planets imprinted on the Edgeworth-Kuiper Belt dust disk. Astron. J. **118**, 580–590 (1999)
Y. Liu, L.A. Taylor, Characterization of lunar dust and a synopsis of available lunar simulants. Planet. Space Sci. **59**(14), 1769–1783 (2011)
Y. Liu, J. Park, D. Schnare, E. Hill, L.A. Taylor, Characterization of lunar dust for toxicological studies. II: Texture and shape characteristics. J. Aerosp. Eng. **21**(4), 272–279 (2008)
P.G. Lucey, M.A. Riner, The optical effects of small iron particles that darken but do not redden: evidence of intense space weathering on Mercury. Icarus **212**, 451–462 (2011)
E.M. MacLennan, H.H. Hsieh, The nucleus of main-belt comet 259P/Garradd. Astrophys. J. Lett. **758**(1), L3 (2012)
M. Makuch, A.V. Krivov, F. Spahn, Long-term dynamical evolution of dusty ejecta from Deimos. Planet. Space Sci. **53**, 357–369 (2005)
I. Mann, Interstellar dust in the solar system. Annu. Rev. Astron. Astrophys. **48**, 173–203 (2010)
F. Marzari, P. Tricarico, H. Scholl, Stability of Jupiter Trojans investigated using frequency map analysis: the MATROS project. Mon. Not. R. Astron. Soc. **345**(4), 1091–1100 (2003)
J.R. Masiero, A.K. Mainzer, J.M. Bauer, T. Grav, C.R. Nugent, R. Stevenson, Asteroid family identification using the hierarchical clustering method and WISE/NEOWISE physical properties. Astrophys. J. **770**, 7 (2013). https://doi.org/10.1088/0004-637X/770/1/7
R.M.E. Mastrapa, R.H. Brown, Ion irradiation of crystalline H_2O-ice: Effect on the 1.65-μm band. Icarus **183**, 207–214 (2006)

T. Matsumoto, A. Tsuchiyama, A. Miyake, T. Noguchi, M. Nakamura, K. Uesugi, A. Takeuchi, Y. Suzuki, T. Nakano, Surface and internal structures of a space-weathered rim of an Itokawa regolith particle. Icarus **257**, 230–238 (2015)
M.K. McClure, C. Espaillat, N. Calvet, E. Bergin, P. D'Alessio, D.M. Watson, P. Manoj, B. Sargent, L.I. Cleeves, Detections of trans-neptunian ice in protoplanetary disks. Astrophys. J. **799**, 162 (2015)
J.E. McCoy, Photometric studies of light scattering above the lunar terminator from Apollo solar corona photography, in *Lunar and Planetary Science Conference Proceedings* (1976), pp. 1087–1112
J.E. McCoy, D.R. Criswell, Evidence for a high altitude distribution of lunar dust. Proc. Lunar Planet. Sci. Conf. **5**, 2991–3005 (1974)
H.J. Melosh, Impact ejection, spallation, and the origin of meteorites. Icarus **59**, 234–260 (1984). https://doi.org/10.1016/0019-1035(84)90026-5
D.A. Mendis, W.I. Axford, Revisiting Iapetus following recent Cassini observations. J. Geophys. Res. **113**, A11 (2008)
F. Merlin, A. Guilbert, C. Dumas, M.A. Barucci, C. de Bergh, P. Vernazza, Properties of the icy surface of the TNO 136108 (2003 EL_{61}). Astron. Astrophys. **466**, 1185–1188 (2007)
P. Michel, W. Benz, D.C. Richardson, Disruption of fragmented parent bodies as the origin of asteroid families. Nature **421**(6923), 608 (2003)
A. Morbidelli, H.F. Levison, R. Gomes, The dynamical structure of the Kuiper belt and its primordial origin, in *The Solar System Beyond Neptune* (2008), pp. 275–292
A. Morbidelli, R. Brasser, R. Gomes, H.F. Levison, K. Tsiganis, Evidence from the asteroid belt for a violent past evolution of Jupiter's orbit. Astron. J. **140**(5), 1391 (2010)
A. Morbidelli, K.J. Walsh, D.P. O'Brien, D.A. Minton, W.F. Bottke, The dynamical evolution of the Asteroid belt, in *Asteroids IV*, ed. by P. Michel, F.E. DeMeo, W.F. Bottke (2015), pp. 493–508
F. Moreno, L. Lara, J. Licandro, J. Ortiz, J. De Léon, V. Alí-Lagoa, B. Agís-González, A. Molina, The dust environment of main-belt comet P/2010 R2 (La Sagra). Astrophys. J. Lett. **738**(1), 16 (2011a)
F. Moreno, J. Licandro, J.L. Ortiz, L.M. Lara, V. Alí-Lagoa, O. Vaduvescu, N. Morales, A. Molina, Z.-Y. Lin, (596) Scheila in outburst: a probable collision event in the Main Asteroid Belt. Astrophys. J. **738**(2), 130 (2011b)
F. Moreno, J. Licandro, A. Cabrera-Lavers, A short-duration event as the cause of dust ejection from main-belt comet P/2012 F5 (Gibbs). Astrophys. J. Lett. **761**(1), 12 (2012)
F. Moreno, A. Cabrera-Lavers, O. Vaduvescu, J. Licandro, F. Pozuelos, The dust environment of main-belt comet P/2012 T1 (PANSTARRS). Astrophys. J. Lett. **770**(2), 30 (2013)
F. Moreno, J. Licandro, C. Álvarez-Iglesias, A. Cabrera-Lavers, F. Pozuelos, Intermittent dust mass loss from activated asteroid P/2013 P5 (PANSTARRS). Astrophys. J. **781**(2), 118 (2014)
F. Moreno, J. Licandro, A. Cabrera-Lavers, F.J. Pozuelos, Dust loss from activated asteroid P/2015 X6. Astrophys. J. **826**(2), 137 (2016a)
F. Moreno, J. Licandro, A. Cabrera-Lavers, F.J. Pozuelos, Early evolution of disrupted asteroid P/2016 G1 (PANSTARRS). Astrophys. J. Lett. **826**, L22 (2016b)
F. Moreno, F.J. Pozuelos, B. Novaković, J. Licandro, A. Cabrera-Lavers, B. Bolin, R. Jedicke, B.J. Gladman, M.T. Bannister, S.D.J. Gwyn, P. Vereš, K. Chambers, S. Chastel, L. Denneau, H. Flewelling, M. Huber, E. Schunová-Lilly, E. Magnier, R. Wainscoat, C. Waters, R. Weryk, D. Farnocchia, M. Micheli, The splitting of double-component active asteroid P/2016 J1 (PANSTARRS). Astrophys. J. Lett. **837**, 3 (2017). https://doi.org/10.3847/2041-8213/aa6036
T.H. Morgan, R.M. Killen, Production mechanisms for faint by possibly detectable coronae about asteroids. Planet. Space Sci. **46**(8), 843–850 (1998)
R.V. Morris, In situ reworking (gardening) of the lunar surface: evidence from the Apollo cores, in *Proc. 9th Lunar Planet. Sci. Conf.* (1978), pp. 1801–1811
N. Murdoch, P. Sánchez, S.R. Schwartz, H. Miyamoto, Asteroid surface geophysics, in *Asteroids IV*, ed. by P. Michel, F.E. DeMeo, W.F. Bottke (2015), pp. 767–792
K. Nagao, R. Okazaki, T. Nakamura, Y.N. Miura, T. Osawa, K.-i. Bajo, S. Matsuda, M. Ebihara, T.R. Ireland, F. Kitajima, H. Naraoka, T. Noguchi, A. Tsuchiyama, H. Yurimoto, M.E. Zolensky, M. Uesugi, K. Shirai, M. Abe, T. Yada, Y. Ishibashi, A. Fujimura, T. Mukai, M. Ueno, T. Okada, M. Yoshikawa, J. Kawaguchi, Irradiation history of Itokawa regolith material deduced from noble gases in the Hayabusa samples. Science **333**, 1128 (2011). https://doi.org/10.1126/science.1207785
A.M. Nakamura, A. Fujiwara, T. Kadono, Velocity of finer fragments from impact. Planet. Space Sci. **42**, 1043–1052 (1994). https://doi.org/10.1016/0032-0633(94)90005-1
T. Nakamura, T. Noguchi, M. Tanaka, M.E. Zolensky, M. Kimura, A. Tsuchiyama, A. Nakato, T. Ogami, H. Ishida, M. Uesugi, T. Yada, K. Shirai, A. Fujimura, R. Okazaki, S.A. Sandford, Y. Ishibashi, M. Abe, T. Okada, M. Ueno, T. Mukai, M. Yoshikawa, J. Kawaguchi, Itokawa dust particles: a direct link between S-type asteroids and ordinary chondrites. Science **333**, 1113 (2011). https://doi.org/10.1126/science.1207758

E. Nakamura, A. Makishima, T. Moriguti, K. Kobayashi, R. Tanaka, T. Kunihiro, T. Tsujimori, C. Sakaguchi, H. Kitagawa, T. Ota, et al., Space environment of an asteroid preserved on micrograins returned by the Hayabusa spacecraft. Proc. Natl. Acad. Sci. **109**(11), 624–629 (2012)
M. Nayak, F. Nimmo, B. Udrea, Effects of mass transfer between Martian satellites on surface geology. Icarus **267**, 220–231 (2016)
D. Nesvorný, P. Jenniskens, H.F. Levison, W.F. Bottke, D. Vokrouhlický, M. Gounelle, Cometary origin of the zodiacal cloud and carbonaceous micrometeorites. Implications for hot debris disks. Astrophys. J. **713**(2), 816 (2010)
D. Nesvorný, D. Janches, D. Vokrouhlický, P. Pokorný, W.F. Bottke, P. Jenniskens, Dynamical model for the zodiacal cloud and sporadic meteors. Astrophys. J. **743**, 129 (2011a)
D. Nesvorný, D. Vokrouhlický, P. Pokorný, D. Janches, Dynamics of dust particles released from Oort Cloud Comets and their contribution to radar meteors. Astrophys. J. **743**, 37 (2011b)
D. Nesvorný, D. Vokrouhlický, R. Deienno, Capture of irregular satellites at Jupiter. Astrophys. J. **784**(1), 22 (2014)
D. Nesvorný, M. Brož, V. Carruba et al., Identification and dynamical properties of asteroid families, in *Asteroids IV* (2015), pp. 297–321
G.A. Neumann, J.F. Cavanaugh, X. Sun, E.M. Mazarico, D.E. Smith, M.T. Zuber, D. Mao, D.A. Paige, S.C. Solomon, C.M. Ernst, O.S. Barnouin, Bright and dark polar deposits on Mercury: evidence for surface volatiles. Science **339**, 296–300 (2013)
T. Nitter, O. Havnes, Dynamics of dust in a plasma sheath and injection of dust into the plasma sheath above Moon and asteroidal surfaces. Earth Moon Planets **56**, 7–34 (1992)
T. Nitter, T.K. Aslaksen, F. Melandsø, O. Havnes, Levitation and dynamics of a collection of dust particles in a fully ionized plasma sheath. IEEE Trans. Plasma Sci. **22**(2), 159–172 (1994)
T. Nitter, O. Havnes, F. Melandsø, Levitation and dynamics of charged dust in the photoelectron sheath above surfaces in space. J. Geophys. Res. **103**(A4), 6605–6620 (1998)
S.K. Noble, C.M. Pieters, L.P. Keller, An experimental approach to understanding the optical effects of space weathering. Icarus **192**, 629–642 (2007)
K. Nogami, M. Fujii, H. Ohashi, Y. Miyachi, S. Sasaki, S. Hasegawa, H. Yano, H. Shibata, T. Iwai, S. Minami, S. Takechi, E. Grün, R. Srama, Development of the Mercury Dust Monitor (MDM) onboard the BepiColombo mission. Planet. Space Sci. **58**, 108–115 (2010)
T. Noguchi, T. Nakamura, M. Kimura, M.E. Zolensky, M. Tanaka, T. Hashimoto, M. Konno, A. Nakato, T. Ogami, A. Fujimura, M. Abe, T. Yada, T. Mukai, M. Ueno, T. Okada, K. Shirai, Y. Ishibashi, R. Okazaki, Incipient space weathering observed on the surface of Itokawa dust particles. Science **333**, 1121 (2011). https://doi.org/10.1126/science.1207794
K.S. Noll, W.M. Grundy, E.I. Chiang, J.-L. Margot, S.D. Kern, Binaries in the Kuiper Belt, in *The Solar System Beyond Neptune*, ed. by M.A. Barucci, H. Boehnhardt, D.P. Cruikshank, A. Morbidelli (University of Arizona Press, Tucson, 2008)
M. Øieroset, D.A. Brain, E. Simpson, D.L. Mitchell, T.D. Phan, J.S. Halekas, R.P. Lin, M.H. Acuña, Search for Phobos and Deimos gas/dust tori using in situ observations from Mars Global Surveyor MAG/ER. Icarus **206**, 189–198 (2010)
N. Onose, A. Fujiwara, Mass-velocity distributions of fragments in oblique impact cratering on gypsum. Meteorit. Planet. Sci. **39**, 321–331 (2004). https://doi.org/10.1111/j.1945-5100.2004.tb00343.x
J. Park, Y. Liu, K.D. Kihm, L.A. Taylor, Characterization of lunar dust for toxicological studies. I: Particle size distribution. J. Aerosp. Eng. **21**(4), 266–271 (2008)
J. Park, B.D. Turrin, G.F. Herzog, F.N. Lindsay, J.S. Delaney, C.C. Swisher, M. Uesugi, Y. Karouji, T. Yada, M. Abe, et al., $^{40}Ar/^{39}Ar$ age of material returned from asteroid 25143 Itokawa. Meteorit. Planet. Sci. **50**(12), 2087–2098 (2015)
M.A. Pelizzari, D.R. Criswell, Lunar dust transport by photoelectric charging at sunset, in *Proc. 9th Lunar Sci. Conf.* (1978), pp. 3225–3237
V. Perera, A.P. Jackson, E. Asphaug, R.-L. Ballouz, The spherical Brazil Nut Effect and its significance to asteroids. Icarus **278**(C), 194–203 (2016)
C.M. Pieters, S.K. Noble, Space weathering on airless bodies. J. Geophys. Res., Planets **121**(1), 1865–1884 (2016)
C.M. Pieters, E.M. Fischer, O. Rode, A. Basu, Optical effects of space weathering: the role of the finest fraction. J. Geophys. Res. **98**(E11), 20817–20824 (1993)
C.M. Pieters, O. Rode, E.M. Fischer, A. Basu, Lunar space weathering and the optical properties of lunar regolith. Astron. Vestn. **28**, 109–119 (1994)
M. Piquette, M. Horányi, The effect of asymmetric surface topography on dust dynamics on airless bodies. Icarus **291**, 65–74 (2017)
P.M. Pires dos Santos, S.M.G. Winter, R. Sfair, D.C. Mourão, Small particles in Pluto's environment: effects of the solar radiation pressure. Mon. Not. R. Astron. Soc. **430**(4), 2761–2767 (2013)

T. Platz, A. Nathues, N. Schorghofer, F. Preusker, E. Mazarico, S.E. Schröder, S. Byrne, T. Kneissl, N. Schmedemann, J.-P. Combe, M. Schäfer, G.S. Thangjam, M. Hoffman, P. Guitierrez-Marques, M.E. Landis, W. Dietrich, J. Ripken, K.-D. Matz, C.T. Russell, Surface water-ice deposits in the northern shadowed regions of Ceres. Nat. Astron. **1**, 7 (2016)
P. Pokorný, D. Vokrouhlický, D. Nesvorný, M. Campbell-Brown, P. Brown, Dynamical model for the toroidal sporadic meteors. Astrophys. J. **789**, 25 (2014)
P. Pokorný, M. Sarantos, D. Janches, Reconciling the Dawn-Dusk Asymmetry in Mercury's Exosphere with the Micrometeoroid Impact Directionality. Astrophys. J. Lett. **842**, 17 (2017). https://doi.org/10.3847/2041-8213/aa775d
A.R. Poppe, Interplanetary dust influx to the Pluto-Charon system. Icarus **246**, 352–359 (2015)
A.R. Poppe, An improved model for interplanetary dust fluxes in the outer Solar System. Icarus **264**, 369–386 (2016)
A. Poppe, M. Horányi, Simulations of the photoelectron sheath and dust levitation on the Lunar surface. J. Geophys. Res. **115**, A08106 (2010)
A. Poppe, M. Horányi, The effect of Nix and Hydra on the putative Pluto-Charon dust cloud. Planet. Space Sci. **59**, 1647–1653 (2011)
A. Poppe, D. James, B. Jacobsmeyer, M. Horányi, First results from the Venetia Burney Student Dust Counter on the New Horizons mission. Geophys. Res. Lett. **37**, L11101 (2010)
A.R. Poppe, M. Piquette, A. Likhanskii, M. Horányi, The effect of surface topography on the lunar photoelectron sheath and electrostatic dust transport. Icarus **221**, 135–146 (2012)
A.R. Poppe, S.M. Curry, S. Fatemi, The Phobos neutral and ionized torus. J. Geophys. Res., Planets **121**(5), 770–783 (2016)
A. Poppe, W. Farrell, J. Halekas, Formation timescales of amorphous rims on lunar grains derived from Artemis observations. J. Geophys. Res., Planets **123**, 37–46 (2018)
C.C. Porco, et al., Cassini observes the active south pole of Enceladus. Science **311**, 1393–1401 (2006)
S.B. Porter, W.M. Grundy, Ejecta transfer in the Pluto system. Icarus **246**, 360–368 (2015)
S.B. Porter, S.J. Desch, J.C. Cook, Micrometeorite impact annealing of ice in the outer Solar System. Icarus **208**, 492–498 (2010)
F.J. Pozuelos, A. Cabrera-Lavers, J. Licandro, F. Moreno, On the dust environment of Main-Belt comet 313 P/Gibbs. Astrophys. J. **806**, 102 (2015)
P. Pravec, D. Vokrouhlický, D. Polishook, D.J. Scheeres, A.W. Harris, A. Galád, O. Vaduvescu, F. Pozo, A. Barr, P. Longa, F. Vachier, F. Colas, D.P. Pray, J. Pollock, D. Reichart, K. Ivarsen, J. Haislip, A. LaCluyze, P. Kušnirák, T. Henych, F. Marchis, B. Macomber, S.A. Jacobson, Y.N. Krugly, A.V. Sergeev, A. Leroy, Formation of asteroid pairs by rotational fission. Nature **466**(7), 1085–1088 (2010)
D. Prialnik, E.D. Rosenberg, Can ice survive in main-belt comets? Long-term evolution models of comet 133P/Elst-Pizarro. Mon. Not. R. Astron. Soc. Lett. **399**(1), 79–83 (2009)
J.J. Rennilson, D.R. Criswell, Surveyor observations of lunar horizon-glow. Moon **10**, 121–142 (1974). https://doi.org/10.1007/BF00655715
J.E. Richardson, H.J. Melosh, R.J. Greenberg, D.P. O'Brien, The global effects of impact-induced seismic activity on fractured asteroid surface morphology. Icarus **179**(2), 325–349 (2005)
D.P. Rubincam, Radiative spin-up and spin-down of small asteroids. Icarus **148**(1), 2–11 (2000)
G.O. Ryabova, The mass of the Geminid meteoroid stream. Planet. Space Sci. **143**, 125–131 (2017)
M. Sachse, J. Schmidt, S. Kempf, F. Spahn, Correlation between speed and size for ejecta from hypervelocity impacts. J. Geophys. Res., Planets **120**, 1847–1858 (2015). https://doi.org/10.1002/2015JE004844
M. Sarantos, R.M. Killen, D.A. Glenar, M. Benna, T.J. Stubbs, Metallic species, oxygen and silicon in the lunar exosphere: upper limits and prospects for LADEE measurements. J. Geophys. Res. **117**, A03103 (2012)
K. Sauer, K. Baumgärtel, U. Motschmann, Phobos events as precursors of solar wind-dust interaction. Geophys. Res. Lett. **20**(2), 165–168 (1993)
B. Schläppi, K. Altwegg, P. Wurz, Asteroid exosphere: a simulation for the ROSETTA flyby targets (2867) Steins and (21) Lutetia. Icarus **195**, 674–685 (2008)
J. Schmidt, N. Brilliantov, F. Spahn, S. Kempf, Slow dust in Enceladus' plume from condensation and wall collisions in tiger stripe fractures. Nature **451**, 685–688 (2008). https://doi.org/10.1038/nature06491
N. Schorghofer, The lifetime of ice on main belt asteroids. Astrophys. J. **682**(1), 697 (2008)
N. Schorghofer, Predictions of depth-to-ice on asteroids based on an asynchronous model of temperature, impact stirring, and ice loss. Icarus **276**, 88–95 (2016)
J. Schwan, X. Wang, H.W. Hsu, E. Grün, M. Horanyi, The charge state of electrostatically transported dust on regolith surfaces. Geophys. Res. Lett. **44**(7), 3059–3065 (2017)
F. Scipioni, F. Tosi, K. Stephan, G. Filacchione, M. Ciarniello, F. Capaccioni, P. Cerroni (The VIMS Team), Spectroscopic classification of icy satellites of Saturn I: identification of terrain units on Dione. Icarus **226**, 1331–1349 (2013)

F. Scipioni, F. Tosi, K. Stephan, G. Filacchione, M. Ciarniello, F. Capaccioni, P. Cerroni (The VIMS Team), Spectroscopic classification of icy satellites of Saturn II: identification of terrain units on Rhea. Icarus **234**, 1–16 (2014)

A.B. Severny, E.I. Terez, A.M. Zvereva, The measurements of sky brightness on Lunokhod-2. Earth Moon Planets **14**(1), 123–128 (1975)

R. Sfair, S.M.G. Winter, Orbital evolution of the μ and ν dust ring particles of Uranus. Astron. Astrophys. **505**, 845–852 (2009)

S.S. Sheppard, C. Trujillo, Discovery and characteristics of the rapidly rotating active asteroid (62412) 2000 SY178 in the main belt. Astron. J. **149**(2), 44 (2015)

Y. Shkuratov, V. Kaydash, V. Korokhin, Y. Velikodsky, N. Opanasenko, G. Videen, Optical measurements of the Moon as a tool to study its surface. Planet. Space Sci. **59**(13), 1326–1371 (2011)

M.R. Showalter, D.P. Hamilton, P.D. Nicholson, A deep search for martian dust rings and inner moons using the Hubble Space Telescope. Planet. Space Sci. **54**, 844–854 (2006)

A.P. Showman, R. Malhotra, The Galilean satellites. Science **296**, 77–84 (1999)

A. Shu, A. Collette, K. Drake, E. Grün, M. Horanyi, S. Kempf, A. Mocker, T. Munsat, P. Northway, R. Srama, Z. Sternovsky, E. Thomas, 3 MV hypervelocity dust accelerator at the Colorado Center for Lunar Dust and Atmospheric Studies. Rev. Sci. Instrum. **83**(7), 075108 (2012)

M. Siegler, R.S. Miller, J.T. Keane, M. Laneuville, D.A. Paige, I. Matsuyama, D.J. Lawrence, A. Crotts, M.J. Poston, Lunar true polar wander inferred from polar hydrogen. Nature **531**(7), 480–484 (2016)

B.A. Smith, et al., The Galilean satellites and Jupiter: Voyager 2 imaging science results. Science **206**, 927–950 (1979a)

B.A. Smith, et al., The Jupiter system through the eyes of Voyager 1. Science **204**, 951–972 (1979b)

B.A. Smith, et al., Voyager 2 in the Uranian system: imaging science results. Science **233**(4759), 43–64 (1986)

S.M. Smith, J.K. Wilson, J. Baumgardner, M. Mendillo, Discovery of the distant lunar sodium tail and its enhancement following the Leonid meteor shower of 1998. Geophys. Res. Lett. **26**(12), 1649–1652 (1999)

C. Snodgrass, C. Tubiana, J.-B. Vincent, H. Sierks, S. Hviid, R. Moissl, H. Boehnhardt, C. Barbieri, D. Koschny, P. Lamy, et al., A collision in 2009 as the origin of the debris trail of asteroid P/2010 A2. Nature **467**(7317), 814–816 (2010)

C. Snodgrass, G.H. Jones, H. Boehnhardt, A. Gibbings, M. Homeister, N. Andre, P. Beck, M.S. Bentley, I. Bertini, N. Bowles, M.T. Capria, C. Carr, M. Ceriotti, A.J. Coates, V.D. Corte, K.L.D. Hanna, A. Fitzsimmons, P.J. Gutierrez, O.R. Hainaut, A. Herique, M. Hilchenbach, H.H. Hsieh, E. Jehin, O. Karatekin, W. Kofman, L.M. Lara, K. Laudan, J. Licandro, S.C. Lowry, F. Marzari, A. Masters, K.J. Meech, F. Moreno, A. Morse, R. Orosei, A. Pack, D. Plettemeier, D. Prialnik, A. Rotundi, M. Rubin, J.P. Sanchez, S. Sheridan, M. Trieloff, A. Winterboer, The Castalia mission to main belt comet 133p/Elst-Pizarro. Adv. Space Res. (2017). https://doi.org/10.1016/j.asr.2017.09.011. http://www.sciencedirect.com/science/article/pii/S0273117717306622

S. Soter, The dust belts of Mars. Cornell Center Radiophys. Space Phys. Rept. 472 (1971)

F. Spahn, et al., Cassini dust measurements at Enceladus and implications for the origin of the E ring. Science **311**, 1416–1418 (2006)

F. Spahn, J. Schmidt, N. Albers, M. Hörning, M. Makuch, M. Seiß, S. Kempf, R. Srama, V. Dikarev, S. Helfert, G. Moragas-Klostermeyer, A.V. Krivov, M. Sremčević, A.J. Tuzzolino, T. Economou, E. Grün, Cassini dust measurements at Enceladus and implications for the origin of the E ring. Science **311**, 1416–1418 (2006a). https://doi.org/10.1126/science.1121375

F. Spahn, N. Albers, M. Hörning, S. Kempf, A.V. Krivov, M. Makuch, J. Schmidt, M. Seiß, M. Sremčević, E ring dust sources: implications from Cassini's dust measurements. Planet. Space Sci. **54**, 1024–1032 (2006b). https://doi.org/10.1016/j.pss.2006.05.022

E.J. Speyerer, R.Z. Povilaitis, M.S. Robinson, P.C. Thomas, R.V. Wagner, Quantifying crater production and regolith overturn on the Moon with temporal imaging. Nature Publishing Group **538**(7624), 215–218 (2016)

M. Sremčević, A.V. Krivov, F. Spahn, Impact-generated dust clouds around planetary satellites: asymmetry effects. Planet. Space Sci. **51**, 455–471 (2003)

M. Sremčević, A.V. Krivov, H. Krüger, F. Spahn, Impact-generated dust clouds around planetary satellites: model versus Galileo data. Planet. Space Sci. **53**, 625–641 (2005). https://doi.org/10.1016/j.pss.2004.10.001

A.J. Steffl, S.A. Stern, First constraints on rings in the Pluto system. Astron. J. **133**, 1485–1489 (2007)

V.J. Sterken, N. Altobelli, S. Kempf, G. Schwehm, R. Srama, E. Grün, The flow of interstellar dust into the solar system. Astron. Astrophys. **538**, A102 (2012)

V.J. Sterken, P. Strub, H. Krüger, R. von Steiger, P.C. Frisch, Sixteen years of Ulysses interstellar dust measurements in the Solar System. III. Simulations and data unveil new insights into local interstellar dust. Astrophys. J. **812**(2), 1–24 (2015)
S.A. Stern, Collisional time scales in the Kuiper Disk and their implications. Astron. J. **110**(2), 856 (1995)
S.A. Stern, Signatures of collisions in the Kuiper Disk. Astron. Astrophys. **310**, 999–1010 (1996)
S.A. Stern, The Lunar atmosphere: history, status, current problems, and context. Rev. Geophys. **37**(4), 453–491 (1999)
S.A. Stern, Ejecta exchange and satellite color evolution in the Pluto system, with implications for KBOs and asteroids with satellites. Icarus **199**, 571–573 (2009)
S.A. Stern, J.E. Colwell, Collisional erosion in the primordial Edgeworth-Kuiper Belt and the generation of the 3050 AU Kuiper Gap. Astrophys. J. **490**, 879–882 (1997)
P. Strub, H. Krüger, V.J. Sterken, Sixteen years of Ulysses interstellar dust measurements in the Solar System. II. Fluctuations in the dust flow from the data. Astrophys. J. **812**(2), 140 (2015)
K.-L. Sun, M. Seiß, M.M. Hedman, F. Spahn, Dust in the arcs of Methone and Anthe. Icarus **284**, 206–215 (2017)
J.R. Szalay, M. Horányi, Annual variation and synodic modulation of the sporadic meteoroid flux to the Moon. Geophys. Res. Lett. **42**(24), 10580–10584 (2015a). https://doi.org/10.1002/2015GL066908
J.R. Szalay, M. Horányi, The search for electrostatically lofted grains above the Moon with the Lunar Dust Experiment. Geophys. Res. Lett. **42**(13), 5141–5146 (2015b). https://doi.org/10.1002/2015GL064324
J.R. Szalay, M. Horányi, Detecting meteoroid streams with an in-situ dust detector above an airless body. Icarus **275**, 221–231 (2016a). https://doi.org/10.1016/j.icarus.2016.04.024
J.R. Szalay, M. Horányi, Lunar meteoritic gardening rate derived from in situ LADEE/LDEX measurements. Geophys. Res. Lett. **43**(10), 4893–4898 (2016b). https://doi.org/10.1002/2016GL069148
J.R. Szalay, M. Horányi, The impact ejecta environment of near Earth asteroids. Astrophys. J. Lett. **830**(2), 29 (2016c). https://doi.org/10.3847/2041-8205/830/2/L29
J.R. Szalay, M. Piquette, M. Horányi, The Student Dust Counter: status report at 23 AU. Earth Planets Space **65**, 1145–1149 (2013). https://doi.org/10.5047/eps.2013.02.005
J.R. Szalay, M. Horányi, A. Colaprete, M. Sarantos, Meteoritic influence on sodium and potassium abundance in the lunar exosphere measured by LADEE. Geophys. Res. Lett. (2016). https://doi.org/10.1002/2016GL069541
J.R. Szalay, P. Pokorný, P. Jenniskens, M. Horanyi, Activity of the 2013 Geminid meteoroid stream at the Moon. Mon. Not. R. Astron. Soc. **474**(3), 4225–4231 (2018)
S. Takasawa, A.M. Nakamura, T. Kadono, M. Arakawa, K. Dohi, S. Ohno, Y. Seto, M. Maeda, K. Shigemori, Y. Hironaka, T. Sakaiya, S. Fujioka, T. Sano, K. Otani, T. Watari, K. Sangen, M. Setoh, N. Machii, T. Takeuchi, Silicate dust size distribution from hypervelocity collisions: implications for dust production in debris disks. Astrophys. J. Lett. **733**, 39 (2011). https://doi.org/10.1088/2041-8205/733/2/L39
D. Tamayo, J.A. Burns, D.P. Hamilton, M.M. Hedman, Finding the trigger to Iapetus' odd global albedo patter: dynamics of dust from Saturn's irregular satellites. Icarus **215**, 260–278 (2011)
M. Tátrallyay, M. Horányi, A. Juhász, J.G. Luhmann, Submicron-sized dust grains in the Martian environment. Adv. Space Res. **12**(9), 927–930 (1992)
S.R. Taylor, *Planetary Science: A Lunar Perspective* (Lunar and Planetary Institute, Houston, 1982)
L.A. Taylor, C.M. Pieters, L.P. Keller, R.V. Morris, D.S. McKay, Lunar mare soils: space weathering and the major effects of surface-correlated nanophase Fe. J. Geophys. Res. **106**(E), 27985–28000 (2001)
L.A. Taylor, C. Pieters, A. Patchen, D.-H.S. Taylor, R.V. Morris, L.P. Keller, D.S. McKay, Mineralogical and chemical characterization of lunar highland soils: insights into the space weathering of soils on airless bodies. J. Geophys. Res. **115**(E), 02002 (2010)
T. Terai, Y. Itoh, Y. Oasa, R. Furusho, J. Watanabe, Photometric measurements of H_2O ice crystallinity on trans-neptunian objects. Astrophys. J. **827**, 65 (2016)
K.-U. Thiessenhusen, A.V. Krivov, H. Krüger, E. Grün, A dust cloud around Pluto and Charon. Planet. Space Sci. **50**, 79–87 (2002)
N. Thomas et al., The morphological diversity of comet 67P/Churyumov-Gerasimenko. Science **347**, 6220 (2015)
H.B. Throop, R.G. French, K. Shoemaker, C.B. Olkin, T.R. Ruhland, L.A. Young, Limits on Pluto's ring system from the June 12 2006 stellar occultation and implications for the New Horizons impact hazard. Icarus **246**, 345–351 (2015)
C.A. Trujillo, M.E. Brown, K.M. Barkume, E.L. Schaller, D.L. Rabinowitz, The surface of 2003 EL_{61} in the near infrared. Astrophys. J. **655**, 1172–1178 (2007)
A. Tsuchiyama, M. Uesugi, T. Matsushima, T. Michikami, T. Kadono, T. Nakamura, K. Uesugi, T. Nakano, S.A. Sandford, R. Noguchi, et al., Three-dimensional structure of Hayabusa samples: origin and evolution of Itokawa regolith. Science **333**(6046), 1125–1128 (2011)

D. Veras, S.A. Jacobson, B.T. Gänsicke, Post-main-sequence debris from rotation-induced YORP break-up of small bodies. Mon. Not. R. Astron. Soc. **445**(3), 2794–2799 (2014). https://doi.org/10.1093/mnras/stu1926.
A.J. Verbiscer, M.F. Skrutskie, D.P. Hamilton, Saturn's largest ring. Nature **461**, 1098–1100 (2009)
J. Veverka et al., Imaging of small-scale features on 433 Eros from NEAR: evidence for a complex regolith. Science **292**, 484 (2001)
C. Vitense, A.V. Krivov, H. Kobayashi, T. Löhne, An improved model of the Edgeworth-Kuiper debris disk. Astron. Astrophys. **540**, A30 (2012)
X. Wang, M. Horányi, S. Robertson, Experiments on dust transport in plasma to investigate the origin of the lunar horizon glow. J. Geophys. Res. **114**, A05103 (2009)
X. Wang, M. Horányi, S. Robertson, Investigation of dust transport on the lunar surface in a laboratory plasma with an electron beam. J. Geophys. Res. **115**, A11102 (2010)
X. Wang, M. Horányi, S. Robertson, Dust transport near electron beam impact and shadow boundaries. Planet. Space Sci. **59**, 1791–1794 (2011)
X. Wang, J. Schwan, H.-W. Hsu, E. Grün, M. Horányi, Dust charging and transport on airless planetary bodies. Geophys. Res. Lett. **43**, 6103–6110 (2016)
B.D. Warner, A.W. Harris, P. Pravec, The asteroid lightcurve database. Icarus **202**(1), 134–146 (2009)
H.A. Weaver, S.A. Stern, M.J. Mutchler, A.J. Steffl, M.W. Buie, W.J. Merline, J.R. Spencer, E.F. Young, L.A. Young, Discovery of two new satellites of Pluto. Nature **439**, 943–945 (2006)
F. Whipple, 1983 TB and the Geminid meteors. International Astronomical Union Circular, No. 3881 (1983)
P. Wiegert, J. Vaubaillon, M. Campbell-Brown, A dynamical model of the sporadic meteoroid complex. Icarus **201**, 295–310 (2009)
S. Yamamoto, T. Mukai, Dust production by impacts of interstellar dust on Edgeworth-Kuiper Belt objects. Astron. Astrophys. **329**, 785–791 (1998)
H. Yano, T. Kubota, H. Miyamoto, T. Okada, D. Scheeres, Y. Takagi, K. Yoshida, M. Abe, S. Abe, O. Barnouin-Jha, et al., Touchdown of the Hayabusa spacecraft at the Muses sea on Itokawa. Science **312**(5778), 1350–1353 (2006)
F. Yoshida, T. Nakamura, Size distribution of faint Jovian l4 Trojan asteroids. Astron. J. **130**(6), 2900 (2005)
M. Yoshikawa, et al., Outline of the next asteroid sample return mission of Japan-Hayabusa-2, in *28th International Symposium on Space Technology and Science* (2011)
M.I. Zimmerman, W.M. Farrell, A. Poppe, Grid-free 2D plasma simulations of the complex interaction between the solar wind and small, near-Earth asteroids. Icarus **238**, 77–85 (2014)
M.I. Zimmerman, W.M. Farrell, C.M. Hartzell, X. Wang, M. Horányi, D.M. Hurley, K. Hibbits, Grain-scale supercharging and breakdown on airless regoliths. J. Geophys. Res., Planets **121**, 2150–2165 (2016)